Enhanced Gαq Signaling in *TSC2*-deficient Cells Is Required for Their Neoplastic Behavior

Aurelie Trefier[1*], Nihad Tousson-Abouelazm[1,2*], Lama Yamani[3], Sajida Ibrahim[4], Kwang-bo Joung [1], Adam Pietrobon[5,6,7], Julien Yockell-Lelievre[5,7], Terence E. Hébert[8], Reese J. Ladak[1], Tomoko Takano[4], Mark Nellist[9], Yoon Namkung[3], David Chatenet[10], William L. Stanford[5,6,7], Stephane A. Laporte [3,8], Arnold S. Kristof[1,11]**

[1] Meakins-Christie Laboratories and Translational Research in Respiratory Diseases Program, Research Institute of the McGill University Health Centre, Faculty of Medicine, Montreal, Quebec, Canada.

[2] Department of Clinical Pharmacology, Faculty of Medicine, Alexandria University, Alexandria, Egypt

[3] Department of Medicine, Research Institute of the McGill University Health Center, McGill University, Montreal, Quebec H4A 3J1, Canada.

[4] Metabolic Disorders and Complications Program, Research Institute of the McGill University Health Centre, Montreal, QC H4A 3J1, Canada

[5] The Sprott Centre for Stem Cell Research, Regenerative Medicine Program, Ottawa Hospital Research Institute, Ottawa, Ontario, Canada.

[6] Department of Cellular and Molecular Medicine, University of Ottawa, Ottawa, Ontario, Canada.

[7] Ottawa Institute of Systems Biology, Ottawa, Ontario, Canada.

[8]Department of Pharmacology and Therapeutics, McGill University, Montréal, QC, H3G 1Y6, Canada.

[9]Department of Clinical Genetics, Erasmus MC, Dr. Molewaterplein 50, 3015 GE Rotterdam, The Netherlands.

[10]Institut National de la Recherche Scientifique, Centre Armand-Frappier Santé Biotechnologie, Groupe de Recherche en Ingénierie des Peptides et en Pharmacothérapie (GRIPP), Université du Québec, Laval, Québec, Canada.

[11] Departments of Critical Care and Medicine, Division of Respirology, McGill University, Montreal, Quebec, Canada

Running Title: Gαq Signaling in Lymphangioleiomyomatosis

**Corresponding author: Arnold S. Kristof, 1001 Décarie Boulevard, EM3.2219, Montreal, Quebec, Canada, H4A 3J1. Tel: 514-934-1934, Fax: 514-933-3962, Email: arnold.Kristof@mcgill.ca

Author contributions

AJRCMB Articles in Press. Published November 08, 2024 as 10.1165/rcmb.2024-0111OC

A.K. conceived of and coordinated the study, and he wrote the manuscript. A.T., N.T., L.Y., K.B., R.L. performed and analyzed the experiments in Figures 1-6. A.P. and J.Y. performed and analyzed the 3D hydrogel migration assay in Fig. 2F and G, in the laboratory of W.L.S. T.T. and S.I. helped design studies on migration and Rho signaling and performed pull-down assays in Fig.5C. As the original creator of the *TSC2* knock out (*TSC2*$^{-/-}$) HEK 293T cells, M.N. provided advice on experimental design as well as validation data. L.Y., Y.N., and S.A.L. provided expert advice on experimental design and constructs, especially for BRET experiments. W.L.S., T.H., D.C. participated in design and/or implementation of experiments, and they provided reagents. All authors reviewed the manuscript and approved the final version.

*These authors contributed equally: Aurelie Trefier and Nihad Tousson-Abouelazm

Sources of funding: The work was supported by the Canadian Institutes for Health Research (CIHR PJT-155-971; PJT-153188) and the LAM Foundation. T.E.H. holds the Canadian Pacific Chair in Biotechnology.

This article has a data supplement, which is accessible at the Supplements tab.

AJRCMB Articles in Press. Published November 08, 2024 as 10.1165/rcmb.2024-0111OC

Abstract

Inherited or sporadic loss of the *TSC2* gene can lead to pulmonary lymphangioleiomyomatosis (LAM), a rare cystic lung disease caused by protease-secreting interstitial tumor nodules. The nodules arise by metastasis of cells that exhibit features of neural crest and smooth muscle lineage ('LAM cells'). Their aberrant growth is attributed to increased activity of 'mechanistic target of rapamycin complex 1' (mTORC1), an anabolic protein kinase that is normally suppressed by the TSC1-TSC2 protein complex. The mTORC1 inhibitor rapamycin slows the progression of LAM, but fails to eradicate disease, indicating a role for mTORC1-independent mechanisms in LAM pathogenesis. Our previous studies revealed G-protein coupled urotensin-II receptor (UT) signaling as a candidate mechanism, but how it promotes oncogenic signaling in *TSC2*-deficient cells remained unknown. Using a human pluripotent stem cell-derived *in vitro* model of LAM, we now show hyperactivation of UT, which was required for their enhanced migration and pro-neoplastic signaling in a rapamycin-insensitive mechanism that required heterotrimeric Gαq/11 (Gαq). Bioluminescence resonance energy transfer assays in HEK 293T cells lacking *TSC2* demonstrated selective and enhanced activation of Gαq and its RhoA-associated effectors compared to wild-type control cells. By immunoprecipitation, recombinant UT was physically associated with Gαq and TSC2. The augmented Gαq signaling in *TSC2*-deleted cells was independent of mTOR activity, and associated with increased endosomal targeting of p63RhoGEF, a known RhoA-activating effector of Gαq. These studies identify potential mTORC1-independent pro-neoplastic mechanisms that can be targeted for prevention or eradication of pulmonary and extrapulmonary LAM tumors.

Keywords: Tuberous sclerosis complex, Mechanistic target of rapamycin, Lymphangioleiomyomatosis, Urotensin-II receptor, Gαq.

AJRCMB Articles in Press. Published November 08, 2024 as 10.1165/rcmb.2024-0111OC

Introduction:

Tuberous sclerosis complex (TSC) is an autosomal dominant neurocutaneous disorder caused by mutations in the *TSC1* or *TSC2* gene (1). Clinical features include mesenchymal tumors in multiple organs arising from cells that have undergone 'second hit' somatic inactivation of the remaining wildtype *TSC1* or *TSC2* allele, and that generally occur in adulthood (1, 2). Pulmonary lymphangioleiomyomatosis (LAM) occurs sporadically or in ~1/3 of patients with TSC, and it is caused by low grade neoplastic interstitial nodules (LAM nodules) that lead to progressive cystic destruction of the lung. Abnormal cells that populate LAM nodules (LAM cells) exhibit hyperactivity of the anabolic effector kinase complex 'mechanistic target of rapamycin complex1' (mTORC1) due to loss of its suppressor *TSC2* (3, 4). The mTORC1 inhibitor, rapamycin (sirolimus©), or its analogues (*e.g.*, everolimus©, temserolimus©), can attenuate the growth of pulmonary LAM nodules or extrapulmonary LAM tumors (*e.g.*, angiomyolipoma, AML), but fails to eradicate disease (5-8). This is due to its paradoxical activation of cell survival mechanisms (9-11), and its failure to block mTORC1-independent oncogenic mechanisms (12, 13).

In keeping with the evolving search for druggable mTORC1-independent mechanisms, analyses of LAM tumors from patients revealed neoplastic processes that were unaffected by rapamycin. These include an aberrant differentiation program leading to a neural crest/smooth muscle mesenchymal lineage (14), with increased activity of signaling pathways regulating cell migration, tissue invasion, and cell survival (15). The Rho GTPase was a critical mediator of these rapamycin-resistant processes, and it was required for the neoplastic features of patient-derived LAM cells, as well as those in cell and animal models of *TSC2* deficiency (16, 17). Moreover, pathway analysis of single cell RNA expression in LAM cells from patient biopsies confirmed enrichment of genes in the Rho signaling family, as well as those encoding previously identified rapamycin-resistant signaling intermediates (*e.g.*, WNT/β-catenin, ERK

AJRCMB Articles in Press. Published November 08, 2024 as 10.1165/rcmb.2024-0111OC

mitogen-activated protein kinase) (18). The same mediators of cell metastasis were observed in other studies using patient-derived LAM cells, and reflect increased epithelial-mesenchymal transition, cell migration and cell survival (19-21) (17, 22, 23). To better understand mechanisms of neoplasia in LAM, we focused on potential Rho-activating proteins that are expressed in the neural crest lineage, that were observed in LAM patient biopsy specimens, and that are differentially regulated in cells lacking *TSC2*.

We detected increased levels of the G-protein coupled (GPCR) urotensin-II receptor (UT), and its neuropeptide ligand urotensin-II (U-II) in LAM biopsy specimens (24). In subsequent studies, a UT antagonist, SB-657510, attenuated the migration of transformed rat *TSC2*-deficient cells and the vascular invasion or growth of tumor xenografts (25). Previous studies have shown that ligand-activated UT can recruit and activate G-proteins Gαq/11 (Gαq), Gα12/13 (GNA12/13), and Gαi/o (Gαi), but not Gαs (Gαs) (26). Gαq and Gα12/13 (GNA12/13) can bind directly and activate the Rho guanine nucleotide exchange factors (RhoGEFs) p63RhoGEF and p115RhoGEF, respectively (27-29). Both enhance the activity of RhoA and its effector focal adhesion kinase (FAK), which in turn drives a tissue invasive and pro-survival phenotype (30). Gαq also activates phospholipase Cβ (PLCβ), leading to enhanced protein kinase C (PKC) and ERK activity (31). Together, these studies indicated that UT signaling is likely to play an important role in the pathogenesis of LAM. However, SB657510 alone failed to induce cytotoxicity or tumor regression (25) suggesting that optimized characterization of UT signaling in *TSC2*-deficient cells might identify novel modifiers of disease severity or therapeutic targets.

We hypothesized that loss of *TSC2* enhances oncogenic UT and Gαq activity pro-neoplastic signaling in *TSC2*-deficient cells (12). Using a stem cell-based *in vitro* model of LAM cells, and *TSC2*-deficient HEK293T cells, we demonstrate that UT is required for their mTORC1-independent neoplastic behavior, primarily via the G-protein Gαq and its Rho

AJRCMB Articles in Press. Published November 08, 2024 as 10.1165/rcmb.2024-0111OC

signaling effectors. We also established a selective, physical, and functional link between TSC2, UT, and Gαq that drives Rho GTPase signaling as a novel mechanism of pathogenesis and potential therapeutic target in LAM.

Methods:

Cell culture and reagents: *TSC2*$^{-/-}$ LAM-like smooth muscle (LAM-SM) cells (32, 33) were maintained in smooth muscle growth media in Matrigel-coated plates. HEK 293T cells were cultured in DMEM supplemented with glutamine, penicillin, 100 U/ml, and streptomycin, 100 µg/ml, in the absence (serum-free media) or presence of 10% FBS. *TSC2* knock out (*TSC2*$^{-/-}$) HEK 293T and parental controls (*TSC2*$^{+/+}$) are described in the online supplement. Due to differential senescence in *TSC2*-deficient cells, cultures were not passaged more than once prior to their use for experiments.

Detection and measurement of protein and mRNA transcript levels: Proteins in media supernatants were measured by ELISA, and those in cell lysates or affinity-purified protein complexes were detected by western blot analysis. Immunoprecipitations were performed from whole cell lysates (700-1000 µg protein) as indicated in the online supplement. UT protein levels were evaluated *in situ* by 'in cell ELISA' or by confocal immunofluorescence microscopy. mRNA levels were measured by quantitative PCR. Details are provided in the online supplement.

Cell migration and cytotoxicity: The migration of *TSC2*$^{-/-}$ LAM-SM and *TSC2*$^{+/+}$ control SM cells were assessed in scratch assays by high content live cell imaging as indicated in the online supplement. Assessment of migration by high-content scanning of live cells in 3D lung mimetic hydrogel matrices was described previously (32). For Incucyte cytotoxicity assays, cells exposed to Cytotox green (Sartorius) were imaged over 48 h before evaluation of dead (Cytotox green-positive) or total (mCherry positive) cells. For RNAi experiments in LAM-SM and

AJRCMB Articles in Press. Published November 08, 2024 as 10.1165/rcmb.2024-0111OC

control cells, cytotoxicity was assessed by crystal violet staining. Details are in the online supplement.

Bioluminescence resonance energy transfer (BRET) assays (34): HEK 293T cells were transiently transfected by calcium phosphate coprecipitation. HA-fused UT (1 or 3µg plasmid per 10 cm dish) was co-transfected with plasmids expressing BRET reporters in which recombinant proteins or subcellular targeting sequences were fused to the coelenterazine-activated light emitter RlucII (donor) or the light-induced (acceptor) fluorescence reporter GFP10 or rGFP (see Fig. E3). 'BRET ratio' is the ratio of the light intensity emitted by GFP10 or rGFP over that emitted by RlucII as detected by a microplate reader. Methods and plasmid constructs for BRET reporters are detailed in the online supplement.

RhoA and PLCβ1 activity: RhoA activity was assessed in whole cell lysates by evaluating levels of GTP-bound Rho by ELISA (G-Lisa, Cytoskeleton, Inc.) or by western blot after its affinity purification by binding to the Rho-binding domain of Rhotekin (35). PLC1β activity was evaluated by measuring accumulated inositol 1-phosphate (IP1) levels using homogeneous time-resolved fluorescence (IP-ONE-Gq kit, Cisbio).

Statistics: The medians of grouped data were compared by Wilcoxon ranked sum test or Kruskal Wallis test for >2 experimental groups. For 3D hydrogel migration assays, reference thresholds were calculated for the distance migrated by 90% of control cells (*i.e.*, 10% of cells migrate/invade past this distance threshold); data are the percentage of cells that migrate past the threshold. For BRET assays, concentration/response relationships were evaluated using the log(agonist) *vs.* response (three parameter) model in Prism (Version 10.1) software, with values for change in BRET (ΔBRET) expressed as means ± SEM (36, 37) as reported in the literature. Curves were fit by least squares regression (R-squared > 0.9 for all datasets). Best-fit values for unshared parameters were used to evaluate differences between $TSC2^{+/+}$ *vs.* $TSC2^{-/-}$

AJRCMB Articles in Press. Published November 08, 2024 as 10.1165/rcmb.2024-0111OC

datasets, and values were inferred for maximum effect (Emax) and half maximal effective concentration (EC_{50}).

Results:

Constitutive urotensin receptor (UT) activity and Gαq/11 signaling in TSC2-deficient LAM-like (LAM-SM) cells. We assessed UT and Gαq activity in a previously described human pluripotent stem cell-based *in vitro* model of LAM cells. These neural crest and smooth-muscle-like (LAM-SM) cells recapitulate molecular and functional properties of patient-derived pulmonary or extra pulmonary LAM tumor cells, and their parental lineages can form renal organoids that mimic angiomyolipomas when xenografted into immunodeficient mice (32, 33, 38). UT protein levels were increased in *TSC2*$^{-/-}$ LAM-SM *vs.* *TSC2*$^{+/+}$ controls (Fig. 1A). Increased protein expression was detected in detergent-permeabilized cells (Fig. 1A), as well as by microscopy in the perinuclear region (Fig. 1B), indicating significant cytoplasmic localization. Levels of the UT ligand urotensin-II (U-II) were also increased in the media supernatants of *TSC2*$^{-/-}$ cells *vs.* those of *TSC*$^{+/+}$ controls (Fig. 1C). Consistent with enhanced cell autonomous UT and Gαq signaling, the phosphorylation of the Rho effector focal adhesion kinase at Tyr·397 (phospho-FAK) was elevated in *TSC2*$^{-/-}$ *vs.* *TSC*$^{+/+}$ cells (Fig. 1D). Protein levels of Gαq were unchanged (Fig. 1D). The levels of urotensin-II receptor (*UTS2R*) and urotensin-II (*UTS2*) mRNA were reduced in *TSC2*$^{-/-}$ cells *vs.* wild-type controls, suggesting a post-transcriptional (*i.e.*, proteostatic) mechanism for the increase in UT and U-II protein levels; known to be increased in LAM or *TSC2*$^{-/-}$ cells (18, 39), *CycD* mRNA levels (positive control) were elevated (Fig. 1E).

In *TSC2*$^{-/-}$ cells, the Gαq and RhoA effector focal adhesion kinase (FAK) exhibited increased phosphorylation in the absence of exogenous ligand (Fig. 2A, B). Its phosphorylation

AJRCMB Articles in Press. Published November 08, 2024 as 10.1165/rcmb.2024-0111OC

was attenuated by the UT antagonists urantide (peptide) and SB-657510 (non-peptide), as well as by the Gαq blocker YM-254890, indicating enhanced constitutive UT and Gαq activity in LAM-SM cells. Incubation with exogenous U-II failed to further enhance cell migration or pFAK levels in *TSC2*$^{-/-}$ cells (Fig. 2C, E1C), suggesting saturation of UT activity. In contrast to its inhibition of FAK activity, YM-254890 *increased* phosphorylation of ERK mitogen-activated protein kinase (ERK) (Fig. 2A, E1D). Rapamycin failed to inhibit the phosphorylation of FAK (Fig. 2A, B), and as shown in other models of *TSC2*-deficiency (40), increased the phosphorylation of ERK (Fig. E1D). Cell migration increased linearly over an 8 h period, was enhanced in *TSC2*$^{-/-}$ cells (Fig. 2C-E), failed to increase with exogenous U-II (Fig. 2C), and was attenuated by UT or Gαq blockade (Fig. 2D); incubation with rapamycin did not significantly affect cell migration (Fig. 2E). In a cell migration/invasion assay using lung tissue-mimetic hydrogel with cleavable MMP2 substrate (described in (32, 41)), YM-254890 or urantide blocked cell migration/matrix invasion, and there was no additional effect of rapamycin (Fig. 2F, G). At low concentrations, the anti-migratory effects of Gαq or UT inhibition were more pronounced in LAM-SM cells (Fig. 2D, F, G). These observations indicate that UT/Gαq activity is required for rapamycin-insensitive increases in phosphorylated FAK levels and cell migration observed in LAM-SM cells.

Effect of UT and Gαq inhibitors on the survival of LAM-SM cells. Given the enhanced Gαq-dependent signaling in *TSC2*$^{-/-}$ cells, and its previously described pro-survival roles in other tumors (42-44), we evaluated whether Gαq blockade facilitates cell death in LAM-SM cells. By high content live cell imaging, and as previously described (reviewed in (45)), the rate of cell death was increased in *TSC2*$^{-/-}$ LAM-SM cells *vs.* wild-type cells (Fig. 2H, I). The Gαq inhibitor YM-254890 or the UT blocker urantide alone were not cytotoxic in *TSC2*$^{-/-}$ cells (Fig. 2H, I). When the ERK inhibitor PD-184252 was added to antagonize YM-254890- or urantide-

AJRCMB Articles in Press. Published November 08, 2024 as 10.1165/rcmb.2024-0111OC

induced increase in ERK activity (Fig. 2A, E1D), there was a >50% increase in cell death (Fig. 2H, I). In contrast to pharmacological Gαq inhibition, depletion of Gαq by RNAi was cytotoxic in *TSC2*$^{+/+}$ or *TSC2*$^{-/-}$ cells by crystal violet staining (Fig 2J), and there was no independent or additive effect of PD-184252. These data indicate a pro-survival role for Gαq signaling in a pre-clinical cell culture model of LAM, and the potential for pharmacological blockade of cell survival by dual inhibition of Gαq and ERK activity.

Selective and enhanced Gαq activation in TSC2-deficient HEK 293T cells exposed to urotensin-II: To better define the mechanism by which UT and Gαq activity are increased in *TSC2*-deficient cells, we adapted bioluminescence resonance energy transfer (BRET) assays in *TSC2* knockout (*TSC2*$^{-/-}$) HEK 293T cells (Fig. E2A, B) versus their isogenic parental controls (*TSC2*$^{+/+}$), each expressing recombinant UT. Given the lack of endogenous expression of UT in HEK 293T cells, we first determined the concentrations of expression plasmids required to achieve equal levels of UT protein in *TSC2*$^{+/+}$ and *TSC2*$^{-/-}$ cells, respectively (Fig. E2C). Using a previously characterized polycistronic expression construct (36), we next co-expressed Gαq-RlucII (donor), GFP10-Gγ (acceptor), and Flag-Gβ with recombinant UT; the ligand-induced decrease in BRET signal observed in cells exposed to U-II reflects activation of the G-protein complex (*i.e.*, dissociation of Gγ from Gαq; Fig. E3A). Exposure of *TSC2*$^{+/+}$ cells expressing UT to U-II led to a concentration-dependent increase in Gαq activity (Fig. 3A, blue). The maximal Gαq activity (*i.e.*, maximum effect, Emax) was significantly increased in *TSC2*$^{-/-}$ vs. wild-type cells (Fig. 3A-C, red). The concentration of U-II required for 50% maximum activation of Gαq (EC_{50}) was similar in *TSC2*$^{+/+}$ and *TSC2*$^{-/-}$ cells (25 nM), suggesting no changes in receptor affinities for U-II. In both *TSC2*$^{+/+}$ and *TSC2*$^{-/-}$ cells, activation of Gαq was abolished by YM-254890 (Fig. 3B), and it was attenuated by the peptide UT antagonist urantide (Fig. 3C). Unlike in rat or human transformed *TSC2*$^{-/-}$ cells or

AJRCMB Articles in Press. Published November 08, 2024 as 10.1165/rcmb.2024-0111OC

tumors (25), and consistent with previous studies using recombinant human UT (46), the UT antagonist SB-657510 had little effect on Gαq activation (Fig. 3C). Neither acute (Fig. E4A) nor long-term (Fig. E4B) exposure to the mTORC1 inhibitor rapamycin, or to the dual mTORC1 and mTORC2 inhibitor Torin1, significantly attenuated Gαq activation by U-II in *TSC2*$^{+/+}$ cells. There was a small reduction of Gαq activation by Torin1, but not rapamycin, in *TSC2*$^{-/-}$ cells. Consistent with an mTORC1-independent effect of Gαq on cell migration (Fig. 2), mTORC1 inhibitors failed to block agonist induced Gαq activity (Fig. E4A, B). As expected, both rapamycin and Torin1 blocked the phosphorylation of S6K at threonine 389, and Torin1 attenuated the phosphorylation of AKT at serine 473 (Fig. E4C-F).

Consistent with other studies investigating UT (47), activation of Gαs by U-II was not significantly increased (Fig. 3D). In control experiments, however, Gαs could be activated by arginine vasopressin (AVP) in cells expressing the AVP receptor (V2R), and there was no effect of *TSC2* loss (Fig 3E). The other Rho-activating G-protein, Gα13, was not induced by U-II in cells expressing UT (Fig. 3F). Albeit to a lesser extent than Gαq, Gαi could be activated by U-II, but only in *TSC2*$^{-/-}$ cells (Fig. 3G, red). Control experiments demonstrated robust activation of Gαi by serum-derived factor-1 in HEK 293T cells expressing its receptor CXCR4; this was, as expected, abolished by the Gαi inhibitor *Pertussis* toxin (PTX) (Fig. 3H). Like V2R and Gαs, CXCR4 activation of Gαi was unaffected by loss of *TSC2* (Fig. 3H). These experiments demonstrate enhanced, selective, and mTOR-independent activation of Gαq in U-II-stimulated *TSC2*$^{-/-}$ versus *TSC2*$^{+/+}$ HEK 293T cells.

Consistent with previous studies (25, 47), activation of recombinant UT by U-II led to the phosphorylation of ERK, and this was increased in *TSC2*$^{-/-}$ HEK 293T cells (Fig. 3I, J; summarized data in Fig. E5A, B). As was the case for Gαq activity (Fig 3B, C), U-II-induced phosphorylation of ERK was blocked by YM-254890 or urantide. Neither U-II, YM-254890, nor urantide significantly influenced phosphorylation of the mTORC1 effector p70S6 kinase

AJRCMB Articles in Press. Published November 08, 2024 as 10.1165/rcmb.2024-0111OC

(S6K) (Fig. 3I, J; E5A, B). These experiments indicate a functional interaction between UT and Gαq that controls canonical Gαq effector pathways, which is enhanced in cells lacking *TSC2*.

Physical association between TSC2, Gαq and UT: Since UT and Gαq activity are increased in TSC2-deficient cells, we next determined whether TSC2, UT, and Gαq are physically associated. A Flag-TSC2 fusion protein (Flag-TSC2) was co-expressed with HA-fused UT (HA-UT) in *TSC2*$^{-/-}$ HEK 293T cells exposed to vehicle or U-II for 5 min. Endogenous Gαq and TSC1, as well as recombinant HA-UT, were enriched in Flag-TSC2 immunoprecipitates by western blot analysis (Fig. 4A). Similarly, in *TSC2*$^{+/+}$ cells expressing Flag-UT, endogenous TSC2 and Gαq were enriched in Flag-UT immunoprecipitates (Fig. 4B). Enrichment of TSC1 in Flag-UT immunoprecipitates was observed in *TSC2*$^{-/-}$ cells exposed to U-II, but not in *TSC2*$^{+/+}$ controls (Fig. 4B). Finally, Flag-UT, and Gαq were detected in endogenous TSC2 immunoprecipitates (Fig. 4C); expression of Flag-UT was required for the interaction between TSC2 and Gαq, but not for that with TSC1. Under these catabolic conditions, enrichment of mTOR was not detected in UT or TSC2 immunoprecipitates (Fig. 4A-C). These results indicate qualitative but specific physical interactions between TSC2, Gαq, and UT.

Enhanced activation of Gαq effectors in TSC2-deficient cells. Gαq binds and activates p63RhoGEF (28) and phospholipase C-beta (PLCβ) (29), which respectively activate RhoA and the production of second messengers diacylglycerol (DAG) and inositol phosphate production (IP3) (48, 49). Recombinant UT was therefore co-expressed with BRET sensors of either RhoA or protein kinase C activity (see Fig. E3B, C). Like Gαq (Fig. 3), Maximal activation of the Rho biosensor was significantly increased in *TSC2*$^{-/-}$ cells (Fig. 5A). By ELISA, endogenous RhoA activity was increased 5 min after exposure to U-II, and RhoA

AJRCMB Articles in Press. Published November 08, 2024 as 10.1165/rcmb.2024-0111OC

induction was higher in *TSC2*$^{-/-}$ (62% increase) vs. *TSC2*$^{+/+}$ cells (24% increase) (Fig. 5B). RhoA activation was blocked by the Gαq inhibitor YM-254890, but not by rapamycin. Enhanced activation of endogenous RhoA (20% and 77% increase in *TSC2*$^{+/+}$ and *TSC2*$^{-/-}$ cells, respectively) was confirmed by GTP-Rho pulldown with the GST-fused Rho binding domain of rhotekin, and subsequent detection of GTP-RhoA and total RhoA by western blot (Fig. 5C). Also consistent with increased Gαq activation in *TSC2*$^{-/-}$ cells, there was a significant increase in PLCβ activity as measured by inositol phosphate-1 accumulation after exposure to U-II (Fig. 5D) (50), as well as protein kinase C (PKC) activation as assessed by its BRET biosensor (Fig. 5F). The increases in PLCβ activity (Fig. 5E), and Rho or PKC BRET biosensor induction (Table E6), by U-II, were abolished by the Gαq inhibitor YM-254890. The lack of residual PLCβ1 or Rho activity in cells exposed to YM-254890 (Fig. 5B, E; Table E6), as well as failure to engage the Gα13 BRET reporter (Fig. 3F), is consistent with an absent or minimal role for Gα13 in UT oncogenic signaling. The UT antagonist urantide inhibited Rho or PKC reporter activity (Table E6), but not PLCβ activity, suggesting preferential antagonism of Rho activation (Fig. 5E). The MEK/ERK inhibitor PD-184352 attenuated PKC reporter activation, but it failed to block Rho reporter activation by U-II (Table E6). Although Gαi activation by U-II was marginally increased in *TSC2*$^{-/-}$ cells (Fig. 3G), Rho reporter activation was unaffected by its antagonist *B. pertussis* toxin (PTX; Table E6).

As was the case for Gαq activity, Rho biosensor induction was not inhibited by rapamycin or Torin1; in fact, it was enhanced during long-term exposure in *TSC2*$^{-/-}$ cells (Fig. 5G). Exposure to rapamycin for 1 h abolished phosphorylation of S6K, but not that of ERK (Fig. 5H, E5C). Together, these results in HEK 293T cells expressing recombinant UT indicate enhanced activation of known Gαq effectors in *TSC2*$^{-/-}$ cells, a requirement for Gαq activity, and resistance to rapamycin.

AJRCMB Articles in Press. Published November 08, 2024 as 10.1165/rcmb.2024-0111OC

Increased endosomal recruitment of p63RhoGEF in TSC2-deficient cells. After GPCR engagement by ligand, Gαq, but not Gα13, can bind and activates p63RhoGEF, a guanine nucleotide exchange factor for RhoA (49). Moreover, sustained Gαq and p63RhoGEF activation have been associated with their persistent localization to the endosomal membrane (37). Given the evidence for Gαq as a primary mediator of *TSC2*-dependent UT activation, we next evaluated whether the amplification of RhoA signaling in *TSC2*-deficient cells is associated with temporal and/or spatial p63RhoGEF activity. $TSC2^{+/+}$ or $TSC2^{-/-}$ HEK 293T cells were co-transfected with plasmids for the expression of UT and p63RhoGEF fused to RlucII, and either rGFP-CAAX (plasma membrane-targeted rGFP) or rGFP-FYVE (endosomal membrane-targeted rGFP, Fig. E3D; described in references (36, 37)). Cells were then exposed to U-II for 5, 30, or 60 min before detection of BRET at the plasma (rGFP-CAAX) or endosomal (rGFP-FYVE) membranes. In cells exposed to U-II for 5 min, we observed dose-dependent recruitment of p63RhoGEF (Fig. 6A) to the plasma membrane, as well as activation of Gαq (Fig. E6A), both of which were increased in $TSC2^{-/-}$ cells. In contrast, there was minimal recruitment of p63RhoGEF to the endosomal membrane at 5 min post-U-II exposure (Fig. 6B). After 30 or 60 min of exposure to U-II, the Emax for p63RhoGEF localization to the plasma membrane decreased with duration of exposure to U-II (Fig. 6C), whereas that for its recruitment to the endosomal membrane increased (Fig. 6D). The Emax for Gαq activation was increased in $TSC2^{-/-}$ compared to $TSC2^{+/+}$ cells, but it was unaffected by the duration of U-II incubation (Fig. E6B). Temporal changes in p63RhoGEF localization were amplified in *TSC2*-deficient versus wild-type cells (Fig. 6C, D), but not those in Gαq activity (Fig. E6B). The EC50 for p63RhoGEF plasma or endosomal membrane recruitment decreased with duration of U-II incubation (*i.e.*, increase in $-\log_{10}$[EC50]), but did not differ between $TSC2^{+/+}$ and $TSC2^{-/-}$ cells (Fig. E6C, D); the same was true for Gαq activation (Fig. S6E). Ligand-dependent membrane localization of p63RhoGEF was blocked by the Gαq

AJRCMB Articles in Press. Published November 08, 2024 as 10.1165/rcmb.2024-0111OC

inhibitor YM-254890 but not by the Gαi inhibitor PTX (Table E7). Finally, as was the case for genetic depletion of *GNAQ* (Fig. 2J), RNAi-mediated depletion of p63RhoGEF mRNA (*ARHGEF25*) was cytotoxic in wild-type and LAM-SM cells (Fig. 6E). These results indicate that the engagement of UT promotes time-dependent localization of recombinant p63RhoGEF to the endosomal compartment that is favored in *TSC2*$^{-/-}$ cells. Moreover, loss of *TSC2* modifies the maximal effect of U-II but does not appear to affect potency (*i.e.*, EC_{50}) of U-II when BRET reporters are used as experimental endpoints. Like Gαq, p63RhoGEF is required for cell survival, and its recruitment to an endosomal compartment requires Gαq activity.

Discussion:

Loss of function mutations in the *TSC2* gene are associated with the aberrant development and neoplastic activity of the abnormal cells (LAM cells) found in pulmonary and extrapulmonary LAM tumors. Because some neoplastic features in LAM are resistant to rapamycin, the identification of mTORC1-independent mechanisms is a priority in the field (13, 51). We focused on the urotensin-II neuropeptide receptor (UT) as a putative autocrine and mTORC1-independent controller of neoplasia in *TSC2*-deficient cells (24, 25). As indicated in Figure 6F, we show that loss of *TSC2* increases constitutive activity of UT and its effector Gαq, and that they are required for the augmented migration and matrix invasion in LAM-SM cells (Fig. 2). Subsequent mechanistic studies in *TSC2* knock out HEK 293T cells also demonstrated enhanced mTOR-independent activation of Gαq (Fig. 3), and its requirement for enhancement of RhoA signaling (Figs. 3, 5). Moreover, we identified the Rho guanine nucleotide exchange factor p63RhoGEF as a Gαq-dependent intermediate involved in the survival of *TSC2*-deficient cells (Fig. 6). Although we could not completely rule out the involvement of G proteins other than Gαq, the near complete blockade of Gαq effectors by the specific Gαq inhibitor YM-254890, the lack of Gα13 activation by UT in BRET assays, and

AJRCMB Articles in Press. Published November 08, 2024 as 10.1165/rcmb.2024-0111OC

the lack of effect of the Gαi inhibitor PTX (Tables E6, E7) all favor a dominant role for Gαq as a key upstream neoplastic mediator in LAM.

Previous studies have also indicated increased mTORC1-independent expression and activity of GPCRs that are known to exhibit a bias towards Gαq signaling. Levels of prostaglandin receptors, as well as cyclooxygenase-2 and its prostaglandin products were elevated in cell and animal models of *TSC2* deficiency (52, 53). Consistent with the neural crest and migratory phenotype of LAM cells, chemokine receptors and their ligands were increased in patient-derived samples (54-56). Increased levels of angiotensin receptor and ligand, as well as an activated renin-angiotensin system, was observed in LAM patient-derived samples and pre-clinical models of *TSC2* deficiency (57, 58). Although other GPCRs have been implicated (56, 59), the above studies support our characterization of Gαq as a key mediator in the mTORC1-independent neoplastic behavior of LAM cells.

The current study reveals potential mechanisms of aberrant GPCR signaling in *TSC2*-deficient cells. The increased UT protein, but not mRNA, levels in LAM-SM cells suggests proteostatic regulation of UT in LAM-SM cells (Fig. 1). Although the translation of mTORC1-sensitive mRNAs as encoded by their 5'-untranslated regions has been extensively studied (60), less is known regarding the selective degradation of proteins in cells lacking *TSC2*. In previous studies, *TSC2*-deficient cells exhibited increased expression of proteosome genes and their encoded proteins (61), as well as those that regulate the unfolded protein response (62); these were proposed as homeostatic transcriptional responses to excessive mTORC1-dependent protein synthesis. In contrast, our identification of physical interactions between TSC2, Gαq, and UT (Fig. 4) supports the possibility that TSC2 coordinates target-selective proteostasis, the mediators of which await further identification in ongoing interactomic studies. One previous study revealed an E3 ligase complex that binds TSC2 and

AJRCMB Articles in Press. Published November 08, 2024 as 10.1165/rcmb.2024-0111OC

reduces its levels (63), but potential TSC2-dependent E3 ligases or deubiquitinases await further identification.

Our experiments in HEK293T cells lacking *TSC2* showed enhanced activation of Gαq and its effectors for equal expression levels of recombinant UT (Fig. 3-6). This was not observed for other interrogated G-proteins (*e.g.*, Gαs, GNA12/13, GNAI1), raising the possibility that amplification of oncogenic G-protein activity is restricted to the subset of GPCRs that are regulated by, or bind, TSC2 and Gαq (Fig. 3, 4). Other candidate mediators of UT/Gαq activity that may be dysregulated in *TSC2*-deficient cells include regulatory proteins (*e.g.*, β-arrestins, GPCR kinases (GRKs), regulator[s] of G-protein signaling (RGS) proteins) that control the expression, activity, or subcellular trafficking of UT and Gαq (49). Consistent with the latter, we found increased vesicular localization of UT and the Gαq-associated RhoA activating protein p63RhoGEF in *TSC2*-deficient cells (Figs. 1, 6). Although we have yet to fully characterize the spatial organization of UT/Gαq signaling in our system, others found that endosomal localization is an important driver of sustained Gαq activity (37).

Gαq is an emerging therapeutic target in cancer (64), and its specific inhibitor YM-254890 allosterically promotes the GDP-bound (inactive) state thus preventing dissociation from its Gβγ subunits (65). Because its depletion by RNAi was cytotoxic, the use of YM-254890 was instrumental in demonstrating that Gαq activity is required for constitutive and ligand-induced pro-neoplastic signaling in LAM-SM and *TSC2*$^{-/-}$ HEK 293T cells, respectively. YM-254890 abolished recruitment and/or activation of RhoA-dependent BRET reporters in HEK 293T cells and blocked the migratory and invasive behavior of LAM-SM cells in physiological relevant nanomolar concentrations. Although Gαq was required for cell survival (Fig. 2), YM-254890 alone was not cytotoxic, in part due to increased ERK pro-survival activity by an unknown mechanism. A similar finding was reported for FAK inhibitors in uveal melanoma cells and tumors, which are also neural crest lineage neoplasias that exhibit

AJRCMB Articles in Press. Published November 08, 2024 as 10.1165/rcmb.2024-0111OC

constitutive Gαq activation and engagement of pro-survival effectors (44, 66). The contribution of Gαq activity to cell survival in LAM-SM cells was reinforced by the increased cytotoxicity observed during its RNAi-mediated depletion of its downstream effector p63RhoGEF (Fig. 6). The biochemical mechanisms by which ERK is activated during exposure to YM-254890 in LAM-SM cells but not in HEK 293T cells is unknown, but may be related to cellular effects of the constitutively saturated UT/Gαq and FAK activation (66) in LAM-SM cells or Gαq-independent hyperactivation of ERK by other signal transduction mechanisms (*e.g.*, integrin engagement by Matrigel-containing cultures). Future studies can characterize and exploit this 'crosstalk' mechanism for the improved design of cytocidal Gαq or combination inhibitors.

In our studies, we leveraged a recently developed pre-clinical *in vitro* model of LAM cells, which was engineered by CRSPR/Cas9 editing *TSC2* in female human pluripotent stem cells (*i.e.*, LAM-SM cells) (32, 38, 67). In addition to the characteristically enhanced activity of mTORC1, LAM-SM cells, or their derived organoid cultures, developed melanocytic markers (*e.g.*, *PMEL*, *MLANA*) and neoplastic behavior (*e.g.*, epithelial to mesenchymal translation) that were resistant to the mTORC1 inhibitor rapamycin (33). Although there may be subtle molecular and phenotypic variation when compared to patient-derived LAM cells, the construct validity of this model is supported by the ability of organoid-derived cells to form tumors in murine xenografts that closely resemble those analyzed in patient biopsies and single cell sequencing studies (33). Using these cells, the current study establishes Gαq as a dominant and mTOR-independent driver of neoplasia in TSC and LAM, and, in conjunction with previous work (32) suggests that LAM-SM cells or tumors might be used to screen for biomarkers or drugs that reflect mTORC1-independent druggable mechanisms of neoplasia in LAM.

AJRCMB Articles in Press. Published November 08, 2024 as 10.1165/rcmb.2024-0111OC

Acknowledgments: We would like to thank Dr. J. Moss for reading the manuscript and advising on the scientific content. The TSC Alliance Biosample Repository hosted at the Van Andel Institute facilitated access to the *TSC2* knockout and parental HEK 293T cells generated at Erasmus MC Department of Clinical Genetics. Clones that were generously provided by Addgene are listed in the online supplement (Table E1). Figure 6F was produced by I. Murawski with Biorender© with copyright agreement.

AJRCMB Articles in Press. Published November 08, 2024 as 10.1165/rcmb.2024-0111OC

References

1. Henske EP, Jozwiak S, Kingswood JC, Sampson JR, Thiele EA. Tuberous sclerosis complex. Nat Rev Dis Primers 2016; 2: 16035.

2. Hasbani DM, Crino PB. Tuberous sclerosis complex. Handb Clin Neurol 2018; 148: 813-822.

3. Tee AR, Manning BD, Roux PP, Cantley LC, Blenis J. Tuberous sclerosis complex gene products, Tuberin and Hamartin, control mTOR signaling by acting as a GTPase-activating protein complex toward Rheb. Curr Biol 2003; 13: 1259-1268.

4. Goncharova EA, Goncharov DA, Eszterhas A, Hunter DS, Glassberg MK, Yeung RS, Walker CL, Noonan D, Kwiatkowski DJ, Chou MM, Panettieri RA, Jr., Krymskaya VP. Tuberin regulates p70 S6 kinase activation and ribosomal protein S6 phosphorylation. A role for the TSC2 tumor suppressor gene in pulmonary lymphangioleiomyomatosis (LAM). J Biol Chem 2002; 277: 30958-30967.

5. Goldberg HJ, Harari S, Cottin V, Rosas IO, Peters E, Biswal S, Cheng Y, Khindri S, Kovarik JM, Ma S, McCormack FX, Henske EP. Everolimus for the treatment of lymphangioleiomyomatosis: a phase II study. Eur Respir J 2015; 46: 783-794.

6. McCormack FX, Inoue Y, Moss J, Singer LG, Strange C, Nakata K, Barker AF, Chapman JT, Brantly ML, Stocks JM, Brown KK, Lynch JP, 3rd, Goldberg HJ, Young LR, Kinder BW, Downey GP, Sullivan EJ, Colby TV, McKay RT, Cohen MM, Korbee L, Taveira-DaSilva AM, Lee HS, Krischer JP, Trapnell BC, National Institutes of Health Rare Lung Diseases C, Group MT. Efficacy and safety of sirolimus in lymphangioleiomyomatosis. N Engl J Med 2011; 364: 1595-1606.

AJRCMB Articles in Press. Published November 08, 2024 as 10.1165/rcmb.2024-0111OC

7. Bissler JJ, Kingswood JC, Radzikowska E, Zonnenberg BA, Frost M, Belousova E, Sauter M, Nonomura N, Brakemeier S, de Vries PJ, Whittemore VH, Chen D, Sahmoud T, Shah G, Lincy J, Lebwohl D, Budde K. Everolimus for angiomyolipoma associated with tuberous sclerosis complex or sporadic lymphangioleiomyomatosis (EXIST-2): a multicentre, randomised, double-blind, placebo-controlled trial. Lancet 2013; 381: 817-824.

8. Bissler JJ, McCormack FX, Young LR, Elwing JM, Chuck G, Leonard JM, Schmithorst VJ, Laor T, Brody AS, Bean J, Salisbury S, Franz DN. Sirolimus for angiomyolipoma in tuberous sclerosis complex or lymphangioleiomyomatosis. N Engl J Med 2008; 358: 140-151.

9. Shah OJ, Wang Z, Hunter T. Inappropriate activation of the TSC/Rheb/mTOR/S6K cassette induces IRS1/2 depletion, insulin resistance, and cell survival deficiencies. Curr Biol 2004; 14: 1650-1656.

10. Manning BD, Logsdon MN, Lipovsky AI, Abbott D, Kwiatkowski DJ, Cantley LC. Feedback inhibition of Akt signaling limits the growth of tumors lacking Tsc2. Genes Dev 2005; 19: 1773-1778.

11. Hung CM, Garcia-Haro L, Sparks CA, Guertin DA. mTOR-dependent cell survival mechanisms. Cold Spring Harb Perspect Biol 2012; 4: a008771.

12. Krymskaya VP, McCormack FX. Lymphangioleiomyomatosis: A Monogenic Model of Malignancy. Annu Rev Med 2017; 68: 69-83.

13. Song X, Cai H, Yang C, Xue X, Wang J, Mo Y, Zhu M, Zhu G, Ye L, Jin M. Possible Novel Therapeutic Targets in Lymphangioleiomyomatosis Treatment. Front Med (Lausanne) 2020; 7: 554134.

AJRCMB Articles in Press. Published November 08, 2024 as 10.1165/rcmb.2024-0111OC

14. Ferrans VJ, Yu ZX, Nelson WK, Valencia JC, Tatsuguchi A, Avila NA, Riemenschn W, Matsui K, Travis WD, Moss J. Lymphangioleiomyomatosis (LAM): a review of clinical and morphological features. J Nippon Med Sch 2000; 67: 311-329.

15. Pietrobon A, Stanford WL. Tuberous Sclerosis Complex Kidney Lesion Pathogenesis: A Developmental Perspective. J Am Soc Nephrol 2023.

16. Goncharova EA, Goncharov DA, Lim PN, Noonan D, Krymskaya VP. Modulation of cell migration and invasiveness by tumor suppressor TSC2 in lymphangioleiomyomatosis. Am J Respir Cell Mol Biol 2006; 34: 473-480.

17. Goncharova EA, Goncharov DA, Li H, Pimtong W, Lu S, Khavin I, Krymskaya VP. mTORC2 is required for proliferation and survival of TSC2-null cells. Mol Cell Biol 2011; 31: 2484-2498.

18. Guo M, Yu JJ, Perl AK, Wikenheiser-Brokamp KA, Riccetti M, Zhang EY, Sudha P, Adam M, Potter A, Kopras EJ, Giannikou K, Potter SS, Sherman S, Hammes SR, Kwiatkowski DJ, Whitsett JA, McCormack FX, Xu Y. Single-Cell Transcriptomic Analysis Identifies a Unique Pulmonary Lymphangioleiomyomatosis Cell. Am J Respir Crit Care Med 2020; 202: 1373-1387.

19. Barnes EA, Kenerson HL, Jiang X, Yeung RS. Tuberin regulates E-cadherin localization: implications in epithelial-mesenchymal transition. Am J Pathol 2010; 177: 1765-1778.

20. Mak BC, Kenerson HL, Aicher LD, Barnes EA, Yeung RS. Aberrant beta-catenin signaling in tuberous sclerosis. Am J Pathol 2005; 167: 107-116.

AJRCMB Articles in Press. Published November 08, 2024 as 10.1165/rcmb.2024-0111OC

21. Gu X, Yu JJ, Ilter D, Blenis N, Henske EP, Blenis J. Integration of mTOR and estrogen-ERK2 signaling in lymphangioleiomyomatosis pathogenesis. Proc Natl Acad Sci U S A 2013; 110: 14960-14965.

22. Astrinidis A, Cash TP, Hunter DS, Walker CL, Chernoff J, Henske EP. Tuberin, the tuberous sclerosis complex 2 tumor suppressor gene product, regulates Rho activation, cell adhesion and migration. Oncogene 2002; 21: 8470-8476.

23. Karbowniczek M, Cash T, Cheung M, Robertson GP, Astrinidis A, Henske EP. Regulation of B-Raf kinase activity by tuberin and Rheb is mammalian target of rapamycin (mTOR)-independent. J Biol Chem 2004; 279: 29930-29937.

24. Kristof AS, You Z, Han YS, Giaid A. Protein expression of urotensin II, urotensin-related peptide and their receptor in the lungs of patients with lymphangioleiomyomatosis. Peptides 2010; 31: 1511-1516.

25. Goldberg AA, Joung KB, Mansuri A, Kang Y, Echavarria R, Nikolajev L, Sun Y, Yu JJ, Laporte SA, Schwertani A, Kristof AS. Oncogenic effects of urotensin-II in cells lacking tuberous sclerosis complex-2. Oncotarget 2016; 7: 61152-61165.

26. Proulx CD, Holleran BJ, Lavigne P, Escher E, Guillemette G, Leduc R. Biological properties and functional determinants of the urotensin II receptor. Peptides 2008; 29: 691-699.

27. Omble A, Kulkarni K. GPCRs that Rhoar the Guanine nucleotide exchange factors. Small GTPases 2022; 13: 84-99.

28. Lutz S, Shankaranarayanan A, Coco C, Ridilla M, Nance MR, Vettel C, Baltus D, Evelyn CR, Neubig RR, Wieland T, Tesmer JJ. Structure of Galphaq-p63RhoGEF-RhoA complex reveals a pathway for the activation of RhoA by GPCRs. Science 2007; 318: 1923-1927.

AJRCMB Articles in Press. Published November 08, 2024 as 10.1165/rcmb.2024-0111OC

29. Rebecchi MJ, Pentyala SN. Structure, function, and control of phosphoinositide-specific phospholipase C. Physiol Rev 2000; 80: 1291-1335.

30. Wu V, Yeerna H, Nohata N, Chiou J, Harismendy O, Raimondi F, Inoue A, Russell RB, Tamayo P, Gutkind JS. Illuminating the Onco-GPCRome: Novel G protein-coupled receptor-driven oncocrine networks and targets for cancer immunotherapy. J Biol Chem 2019; 294: 11062-11086.

31. Lappano R, Maggiolini M. G protein-coupled receptors: novel targets for drug discovery in cancer. Nat Rev Drug Discov 2011; 10: 47-60.

32. Pietrobon A, Yockell-Lelievre J, Melong N, Smith LJ, Delaney SP, Azzam N, Xue C, Merwin N, Lian E, Camacho-Magallanes A, Dore C, Musso G, Julian LM, Kristof AS, Tam RY, Berman JN, Shoichet MS, Stanford WL. Tissue-Engineered Disease Modeling of Lymphangioleiomyomatosis Exposes a Therapeutic Vulnerability to HDAC Inhibition. Adv Sci (Weinh) 2023: e2302611.

33. Pietrobon A, Yockell-Lelievre J, Flood TA, Stanford WL. Renal organoid modeling of tuberous sclerosis complex reveals lesion features arise from diverse developmental processes. Cell Rep 2022; 40: 111048.

34. Namkung Y, Radresa O, Armando S, Devost D, Beautrait A, Le Gouill C, Laporte SA. Quantifying biased signaling in GPCRs using BRET-based biosensors. Methods 2016; 92: 5-10.

35. Zhang H, Cybulsky AV, Aoudjit L, Zhu J, Li H, Lamarche-Vane N, Takano T. Role of Rho-GTPases in complement-mediated glomerular epithelial cell injury. Am J Physiol Renal Physiol 2007; 293: F148-156.

AJRCMB Articles in Press. Published November 08, 2024 as 10.1165/rcmb.2024-0111OC

36. Namkung Y, Le Gouill C, Lukashova V, Kobayashi H, Hogue M, Khoury E, Song M, Bouvier M, Laporte SA. Monitoring G protein-coupled receptor and beta-arrestin trafficking in live cells using enhanced bystander BRET. Nat Commun 2016; 7: 12178.

37. Wright SC, Lukasheva V, Le Gouill C, Kobayashi H, Breton B, Mailhot-Larouche S, Blondel-Tepaz E, Antunes Vieira N, Costa-Neto C, Heroux M, Lambert NA, Parreiras ESLT, Bouvier M. BRET-based effector membrane translocation assay monitors GPCR-promoted and endocytosis-mediated Gq activation at early endosomes. Proc Natl Acad Sci U S A 2021; 118.

38. Delaney SP, Julian LM, Pietrobon A, Yockell-Lelièvre J, Doré C, Wang TT, Doyon VC, Raymond A, Patten DA, Kristof AS, Harper M-E, Sun H, Stanford WL. Human pluripotent stem cell modeling of tuberous sclerosis complex reveals lineage-specific therapeutic vulnerabilities. bioRxiv 2020: 683359.

39. Park JH, Arakawa-Takeuchi S, Jinno S, Okayama H. Rho-associated kinase connects a cell cycle-controlling anchorage signal to the mammalian target of rapamycin pathway. J Biol Chem 2011; 286: 23132-23141.

40. Carracedo A, Ma L, Teruya-Feldstein J, Rojo F, Salmena L, Alimonti A, Egia A, Sasaki AT, Thomas G, Kozma SC, Papa A, Nardella C, Cantley LC, Baselga J, Pandolfi PP. Inhibition of mTORC1 leads to MAPK pathway activation through a PI3K-dependent feedback loop in human cancer. J ClinInvest 2008; 118: 3065-3074.

41. Tam RY, Yockell-Lelievre J, Smith LJ, Julian LM, Baker AEG, Choey C, Hasim MS, Dimitroulakos J, Stanford WL, Shoichet MS. Rationally Designed 3D Hydrogels Model Invasive Lung Diseases Enabling High-Content Drug Screening. Adv Mater 2019; 31: e1806214.

AJRCMB Articles in Press. Published November 08, 2024 as 10.1165/rcmb.2024-0111OC

42. Castillo-Kauil A, Garcia-Jimenez I, Cervantes-Villagrana RD, Adame-Garcia SR, Beltran-Navarro YM, Gutkind JS, Reyes-Cruz G, Vazquez-Prado J. Galphas directly drives PDZ-RhoGEF signaling to Cdc42. J Biol Chem 2020; 295: 16920-16928.

43. Annala S, Feng X, Shridhar N, Eryilmaz F, Patt J, Yang J, Pfeil EM, Cervantes-Villagrana RD, Inoue A, Haberlein F, Slodczyk T, Reher R, Kehraus S, Monteleone S, Schrage R, Heycke N, Rick U, Engel S, Pfeifer A, Kolb P, Konig G, Bunemann M, Tuting T, Vazquez-Prado J, Gutkind JS, Gaffal E, Kostenis E. Direct targeting of Galpha(q) and Galpha(11) oncoproteins in cancer cells. Sci Signal 2019; 12.

44. Feng X, Arang N, Rigiracciolo DC, Lee JS, Yeerna H, Wang Z, Lubrano S, Kishore A, Pachter JA, Konig GM, Maggiolini M, Kostenis E, Schlaepfer DD, Tamayo P, Chen Q, Ruppin E, Gutkind JS. A Platform of Synthetic Lethal Gene Interaction Networks Reveals that the GNAQ Uveal Melanoma Oncogene Controls the Hippo Pathway through FAK. Cancer Cell 2019; 35: 457-472 e455.

45. Henske EP, McCormack FX. Lymphangioleiomyomatosis - a wolf in sheep's clothing. J Clin Invest 2012; 122: 3807-3816.

46. Behm DJ, McAtee JJ, Dodson JW, Neeb MJ, Fries HE, Evans CA, Hernandez RR, Hoffman KD, Harrison SM, Lai JM, Wu C, Aiyar NV, Ohlstein EH, Douglas SA. Palosuran inhibits binding to primate UT receptors in cell membranes but demonstrates differential activity in intact cells and vascular tissues. Br J Pharmacol 2008; 155: 374-386.

47. Vaudry H, Leprince J, Chatenet D, Fournier A, Lambert DG, Le Mevel JC, Ohlstein EH, Schwertani A, Tostivint H, Vaudry D. International Union of Basic and Clinical Pharmacology. XCII. Urotensin II, urotensin II-related peptide, and their receptor: from structure to function. Pharmacol Rev 2015; 67: 214-258.

AJRCMB Articles in Press. Published November 08, 2024 as 10.1165/rcmb.2024-0111OC

48. Namkung Y, LeGouill C, Kumar S, Cao Y, Teixeira LB, Lukasheva V, Giubilaro J, Simoes SC, Longpre JM, Devost D, Hebert TE, Pineyro G, Leduc R, Costa-Neto CM, Bouvier M, Laporte SA. Functional selectivity profiling of the angiotensin II type 1 receptor using pathway-wide BRET signaling sensors. Sci Signal 2018; 11.

49. Sanchez-Fernandez G, Cabezudo S, Garcia-Hoz C, Beninca C, Aragay AM, Mayor F, Jr., Ribas C. Galphaq signalling: the new and the old. Cell Signal 2014; 26: 833-848.

50. Zimmerman B, Beautrait A, Aguila B, Charles R, Escher E, Claing A, Bouvier M, Laporte SA. Differential beta-arrestin-dependent conformational signaling and cellular responses revealed by angiotensin analogs. Sci Signal 2012; 5: ra33.

51. McCarthy C, Gupta N, Johnson SR, Yu JJ, McCormack FX. Lymphangioleiomyomatosis: pathogenesis, clinical features, diagnosis, and management. Lancet Respir Med 2021; 9: 1313-1327.

52. Li C, Lee PS, Sun Y, Gu X, Zhang E, Guo Y, Wu CL, Auricchio N, Priolo C, Li J, Csibi A, Parkhitko A, Morrison T, Planaguma A, Kazani S, Israel E, Xu KF, Henske EP, Blenis J, Levy BD, Kwiatkowski D, Yu JJ. Estradiol and mTORC2 cooperate to enhance prostaglandin biosynthesis and tumorigenesis in TSC2-deficient LAM cells. J Exp Med 2014; 211: 15-28.

53. Li C, Liu X, Liu Y, Zhang E, Medepalli K, Masuda K, Li N, Wikenheiser-Brokamp KA, Osterburg A, Borchers MT, Kopras EJ, Plas DR, Sun J, Franz DN, Capal JK, Mays M, Sun Y, Kwiatkowski DJ, Alayev A, Holz MK, Krueger DA, Siroky BJ, Yu JJ. Tuberin Regulates Prostaglandin Receptor-Mediated Viability, via Rheb, in mTORC1-Hyperactive Cells. Mol Cancer Res 2017; 15: 1318-1330.

AJRCMB Articles in Press. Published November 08, 2024 as 10.1165/rcmb.2024-0111OC

54. Pacheco-Rodriguez G, Kumaki F, Steagall WK, Zhang Y, Ikeda Y, Lin JP, Billings EM, Moss J. Chemokine-enhanced chemotaxis of lymphangioleiomyomatosis cells with mutations in the tumor suppressor TSC2 gene. J Immunol 2009; 182: 1270-1277.

55. Clements D, Markwick LJ, Puri N, Johnson SR. Role of the CXCR4/CXCL12 axis in lymphangioleiomyomatosis and angiomyolipoma. J Immunol 2010; 185: 1812-1821.

56. Le K, Steagall WK, Stylianou M, Pacheco-Rodriguez G, Darling TN, Vaughan M, Moss J. Effect of beta-agonists on LAM progression and treatment. Proc Natl Acad Sci U S A 2018; 115: E944-E953.

57. Valencia JC, Pacheco-Rodriguez G, Carmona AK, Xavier J, Bruneval P, Riemenschneider WK, Ikeda Y, Yu ZX, Ferrans VJ, Moss J. Tissue-specific renin-angiotensin system in pulmonary lymphangioleiomyomatosis. Am J Respir Cell Mol Biol 2006; 35: 40-47.

58. Kreitmann L, Helms J, Martin-Loeches I, Salluh J, Poulakou G, Pene F, Nseir S. ICU-acquired infections in immunocompromised patients. Intensive Care Med 2024.

59. Li F, Zhang Y, Lin Z, Yan L, Liu Q, Li Y, Pei X, Feng Y, Han X, Yang J, Zheng F, Li T, Zhang Y, Fu Z, Shao D, Yu J, Li C. Targeting SPHK1/S1PR3-regulated S-1-P metabolic disorder triggers autophagic cell death in pulmonary lymphangiomyomatosis (LAM). Cell Death Dis 2022; 13: 1065.

60. Roux PP, Topisirovic I. Signaling Pathways Involved in the Regulation of mRNA Translation. Mol Cell Biol 2018; 38.

61. Zhang Y, Nicholatos J, Dreier JR, Ricoult SJ, Widenmaier SB, Hotamisligil GS, Kwiatkowski DJ, Manning BD. Coordinated regulation of protein synthesis and degradation by mTORC1. Nature 2014; 513: 440-443.

AJRCMB Articles in Press. Published November 08, 2024 as 10.1165/rcmb.2024-0111OC

62. Ozcan U, Ozcan L, Yilmaz E, Duvel K, Sahin M, Manning BD, Hotamisligil GS. Loss of the tuberous sclerosis complex tumor suppressors triggers the unfolded protein response to regulate insulin signaling and apoptosis. Mol Cell 2008; 29: 541-551.

63. Hu J, Zacharek S, He YJ, Lee H, Shumway S, Duronio RJ, Xiong Y. WD40 protein FBW5 promotes ubiquitination of tumor suppressor TSC2 by DDB1-CUL4-ROC1 ligase. Genes Dev 2008; 22: 866-871.

64. Campbell AP, Smrcka AV. Targeting G protein-coupled receptor signalling by blocking G proteins. Nat Rev Drug Discov 2018; 17: 789-803.

65. Kostenis E, Pfeil EM, Annala S. Heterotrimeric Gq proteins as therapeutic targets? J Biol Chem 2020; 295: 5206-5215.

66. Paradis JS, Acosta M, Saddawi-Konefka R, Kishore A, Gomes F, Arang N, Tiago M, Coma S, Lubrano S, Wu X, Ford K, Day CP, Merlino G, Mali P, Pachter JA, Sato T, Aplin AE, Gutkind JS. Synthetic Lethal Screens Reveal Cotargeting FAK and MEK as a Multimodal Precision Therapy for GNAQ-Driven Uveal Melanoma. Clin Cancer Res 2021; 27: 3190-3200.

67. Julian LM, Delaney SP, Wang Y, Goldberg AA, Dore C, Yockell-Lelievre J, Tam RY, Giannikou K, McMurray F, Shoichet MS, Harper ME, Henske EP, Kwiatkowski DJ, Darling TN, Moss J, Kristof AS, Stanford WL. Human Pluripotent Stem Cell-Derived TSC2-Haploinsufficient Smooth Muscle Cells Recapitulate Features of Lymphangioleiomyomatosis. Cancer Res 2017; 77: 5491-5502.

AJRCMB Articles in Press. Published November 08, 2024 as 10.1165/rcmb.2024-0111OC

Figure Legends

Figure 1: Urotensin-II receptor (UT) and urotensin-II (U-II) expression in LAM-SM cells: After incubation for 18h in serum-free media, cultures of wild-type (*TSC2*$^{+/+}$) or LAM-like smooth muscle cells (LAM-SM; *TSC2*$^{-/-}$) were evaluated for **A.** Urotensin-II receptor (UT) protein levels by in cell ELISA after exposure to vehicle or 0.5% Triton X-100 for 5min (n=6 performed in octuplicate); **B.** reactivity to anti-UT (red), Phalloidin (stain for F-actin; green), or DAPI (blue) by immunofluorescence confocal microscopy (representative of 3 experiments); **C.** Urotensin-II (U-II) protein levels in media supernatants measured by ELISA (n=3 performed in duplicate); **D.** phosphorylation of focal adhesion kinase (pFAK), total FAK, or Gαq levels; shown are representative western blots (images are composite versions from the same gel) and summarized densitometry data (n=6); **E.** Fold change *vs. TSC2*$^{+/+}$ control in *UTS2*, *UTS2R*, or cyclin D (*CycD*) mRNA levels by quantitative PCR (n=3 performed in duplicate). Medians ± interquartile range are shown in A, C-E. $^{*}p < 0.05$ *vs. TSC2*$^{+/+}$ control, $^{\dagger}p<0.05$ *vs. TSC2*$^{-/-}$ control.

Figure 2: Neoplastic behavior of LAM-SM cells: A. After serum starvation for 18 h, *TSC2*$^{+/+}$ or LAM-SM (*TSC2*$^{-/-}$) cells were exposed to urotensin-II receptor (UT) inhibitors SB-657510 (SB; 100 nM) or urantide (Uran; 100 nM) for 45 minutes, 50 nM rapamycin (Rapa), or the GαQ inhibitor YM-254890 (YM; 200 nM) for 1 h before preparation of whole cell lysates and interrogation of the indicated proteins by western blot analysis, included the phosphorylated (active) or total forms of FAK, S6K, or ERK. **B.** Shown are medians of active FAK band densitometry levels (pFAK/total FAK normalized to *TSC2*$^{+/+}$ untreated control = 1) ± interquartile range, n=3. **C-E:** After serum starvation for 18 h, cell culture surfaces were subjected to a linear scratch, exposure to vehicle or 10 nM urotensin-II (U-II) (**C**), 100 nM urantide or 200 nM YM-254890 (**D**), or 50 nM rapamycin (**E**), followed by high-content imaging of cell migration into the scratch defect for 8 h. Percent confluency (% confluency) is

AJRCMB Articles in Press. Published November 08, 2024 as 10.1165/rcmb.2024-0111OC

the fractional area of the wound that is occupied by cells. Data are the medians of % confluency / h (*i.e.*, rate of migration) *vs.* $TSC2^{+/+}$ control = 1 ± interquartile range (n=5-8). **F.** and **G:** Cells were applied to the surfaces of 3D lung mimetic hydrogel matrices and subjected to live high content confocal imaging for 72h after exposure to vehicle or 50 nM rapamycin, without or with the indicated concentrations of (**F**) YM-254890 or (**G**) urantide. % invasion is the proportion of cells that migrate past a distance threshold determined by the 90th percentile of vehicle-exposed $TSC2^{+/+}$ or $TSC2^{-/-}$ cells. Data are the medians for % invasion from duplicate samples ± interquartile range, n=3. **H.** and **I:** Cells were evaluated by high-content live-cell imaging (Incucyte) as in Figs. 2C-E after incubation with Incucyte Cytotox green and exposure to the indicated concentrations of YM-254890, urantide, or 2 μM PD-184252 (PD). Dead cells accumulating Cytotox green (Cytotox+) were expressed as a proportion of total cells (mCherry+). Data are medians of proportional cell death in octuplet samples ± interquartile range, and they are representative of 3 experiments. **J.** Cells were exposed to lentiviral vectors expressing scrambled shRNAs (Ctrl) or those targeting two distinct sequences in the Gαq messenger RNA transcript (GNAQ_1, GNAQ_2). After 72 h, cells were exposed to vehicle or PD-184352 for 18 h before staining with crystal violet, solubilization, and measurement of light absorbance at 570 nm. Data are the medians of absorbance values ± interquartile range in duplicate samples, and they are representative of 4 individual experiments. *$p<0.05$ *vs.* vehicle treated $TSC2^{+/+}$ control; †$p<0.05$ *vs.* vehicle treated $TSC2^{-/-}$ control; δ $p<0.05$ *vs.* $TSC2^{-/-}$ cells exposed to PD-184252 alone.

Figure 3: Effect of *TSC2*-deficiency on signaling by Gαq effectors in response to UT ligation. Plasmids for the expression of recombinant UT were co-transfected into $TSC2^{+/+}$ or $TSC2^{-/-}$ HEK 293T cells with plasmids for the expression of the indicated BRET G-protein reporters before exposure to agonists and/or antagonists at the indicated concentrations. **A.**

AJRCMB Articles in Press. Published November 08, 2024 as 10.1165/rcmb.2024-0111OC

Concentration-response curves for Gαq activation by the UT agonist U-II (*i.e.*, dissociation from its Gβ and Gγ subunits; see Fig. E3A). Data are expressed as means of ΔBRET ± SEM from 6 experiments each performed in duplicate. **B.** Cells were exposed to vehicle or the Gαq inhibitor YM-254890 (YM; 200 nM) or **C.** the UT inhibitor urantide (Uran; 100 nM) or SB-657510 (SB; 100 nM) for 45 min prior to addition of U-II and detection of BRET signals. Data are medians of maximum effect (Emax) normalized to vehicle control in $TSC2^{+/+}$ cells = 100% ± interquartile range from 3-6 individual experiments. **D-H.** Cells were co-transfected with reporters for Gαs, Gα13, or Gαi before exposure to U-II at the indicated concentrations. In control experiments, the arginine vasopressin (AVP) receptor V2R and the serum-derived factor-1 (SDF-1) receptor CXCR4 were co-transfected with the indicated BRET reporters. In H., cells were also exposed to vehicle or *B. pertussis* toxin (PTX; 100 ng/ml). Data are the means of ΔBRET measurements ± SEM from 3-5 individual experiments each performed in duplicate. **I** and **J**. Cells were transfected with plasmids expressing recombinant UT before exposure to U-II (10 nM), the YM-254890 (200 nM) or urantide (100 nM) before detection of the indicated proteins by western blot analysis. Summarized densitometry data are indicated in Fig. E5A and B. *$p<0.05$ *vs.* $TSC2^{+/+}$.

Figure 4: Physical association between TSC2, Gαq, and UT: $TSC2^{+/+}$ or $TSC2^{-/-}$ HEK 293T cells were transfected with plasmids for the expression of the indicated recombinant Flag- or HA-fused recombinant proteins. **A.** HA-UT and Flag-TSC2 were co-expressed in $TSC2^{-/-}$ cells exposed to 10 nM U-II for 5 min before affinity purification of Flag-containing protein complexes and detection of the indicated proteins by western blot analysis. **B**. Flag-UT was expressed in $TSC2^{+/+}$ or $TSC2^{-/-}$ cells before exposure to vehicle or 10 nM U-II for 5 min and affinity purification of Flag-UT-containing complexes from cell lysates, and detection of the indicated proteins by western blot analysis. **C**. Flag-UT was expressed in $TSC2^{+/+}$ cells before

AJRCMB Articles in Press. Published November 08, 2024 as 10.1165/rcmb.2024-0111OC

exposure to vehicle or 10 nM U-II for 5 min, and immunoprecipitation of cell lysates with anti-TSC2 antibody or IgG control. For each analyte, shown images are from the same gel and exposure. In each case, aliquots of whole cell lysates were saved prior to immunoprecipitation and loaded on the same gel (WCL; left) to validate detection of proteins detected in affinity-purified complexes (IP; right). Data are representative of 3-5 individual experiments.

Figure 5: Effect of *TSC2*-deficiency on activation of Gαq downstream effectors in response to UT ligation. A. *TSC2*$^{+/+}$ or *TSC2*$^{-/-}$ cells were co-transfected with plasmids for expression of HA-UT and a biosensor for RhoA activation (see Fig. E3B). Shown are summarized concentration-response curves for RhoA activation by exposure to the indicated concentrations of U-II (*$p < 0.05$ *vs.* *TSC2*$^{+/+}$). **B.** Cells were exposed to vehicle or 10 nM U-II for 0 or 5 min in the absence or presence of 200 nM YM-254890 (YM) or 50 nM rapamycin (Rapa), before interrogation of cell lysates for GTP-RhoA (*i.e.*, activated RhoA) by ELISA (*$p < 0.05$ *vs.* vehicle control). **C.** In cells exposed to U-II for 0 or 5 min, activation of RhoA was evaluated by GST-Rhotekin affinity purification of GTP-RhoA from whole cell lysates and detection of RhoA by western blot analysis. Data are the medians ± interquartile range of fold changes in ratios of purified GTP-RhoA to total RhoA densitometry with vehicle-treated *TSC2*$^{+/+}$ or *TSC2*$^{-/-}$ controls =1. Representative Western blots (composites from the same gel) are shown with GST alone negative control. **D.** Cells were exposed to the indicated concentrations of U-II, or **E.** vehicle or 10 nM U-II in the absence or presence of 200 nM YM-254890 (YM) or 100 nM urantide (Uran), for 60 min before preparation of lysates and evaluation of inositol 1-phosphate (IP1) levels by homogeneous time-resolved fluorescence. Data are medians ± interquartile range of IP1 levels normalized to vehicle-treated controls = 100%. *$p < 0.05$ *vs.* vehicle control, †$p < 0.05$ *vs.* U-II. **F.** Cells were co-transfected with plasmids for expression of HA-UT and a biosensor of protein kinase C (PKC) activation (see

AJRCMB Articles in Press. Published November 08, 2024 as 10.1165/rcmb.2024-0111OC

Fig. E3C). Shown are summarized concentration-response curves for PKC activation by exposure to the indicated concentrations of U-II (means ± SEM, *p < 0.05 *vs.* *TSC2*$^{+/+}$). **G.** Cells were co-transfected with plasmids for expression of HA-UT and the Rho biosensor (Fig. E3B), before exposure to vehicle, rapamycin (50 nM), or torin-1 (50 nM) for 1 h (left) or 18 h (right), and generation of U-II concentration-response curves as shown in panel A. The maximum effect (Emax) was determined for each curve. Data are the medians of Emax normalized to vehicle-treated controls = 100% ± interquartile range. *p < 0.05 *vs.* *TSC2*$^{+/+}$ vehicle control, †p < 0.05 *vs.* *TSC2*$^{-/-}$ vehicle control. **H.** Cells were transfected with empty vector control, or plasmids for the expression of recombinant UT before exposure to vehicle or 10 nM U-II in the absence or presence of 50 nM rapamycin, and detection of the indicated proteins by western blot analysis. Summarized densitometry data are indicated in Fig. E5C.

Figure. 6: Effect of *TSC2*-deficiency on endosomal targeting of p63RhoGEF in HEK 293T cells: *TSC2*$^{+/+}$ or *TSC2*$^{-/-}$ cells were co-transfected with plasmids for the expression of HA-UT, RlucII-fused p63RhoGEF, and **A.** rGFP-fused CAAX motif (plasma membrane-targeting) or **B.** rGFP-fused FYVE domain (endosomal membrane-targeting) (see Fig. E3D). BRET signals were measured in cells exposed to the indicated concentrations of U-II for 5 min. Also shown are the Emax values for p63RhoGEF recruitment to the **C.** plasma or **D.** endosomal membrane after 5, 30 or 60 min of exposure to U-II. Data are the means of ΔBRET ± SEM from 5-9 experiments or medians of Emax ± interquartile range. *p<0.05 *vs.* *TSC2*$^{+/+}$ control. †p<0.05 *vs.* *TSC2*$^{-/-}$ cells exposed to U-II for 5 min. **E.** *TSC2*$^{+/+}$ or *TSC2*$^{-/-}$ or LAM-SM cells were exposed to lentiviral vectors expressing non-targeting shRNA (Ctrl) or those targeting two distinct sequences in the p63RhoGEF messenger RNA transcript (ARHGEF25_1, ARHGEF25_2) for 72 h. Cells were subjected to crystal violet staining and solubilization for measurement of absorbance at 570 nm. Data are the medians of absorbance values ±

AJRCMB Articles in Press. Published November 08, 2024 as 10.1165/rcmb.2024-0111OC

interquartile range in triplicate samples representative of three individual experiments performed in duplicate. **F.** Summary diagram: TSC2 forms a protein complex with UT and Gαq. Loss of TSC2 is associated with increased UT levels and enhanced Gαq activity. Gαq activity is required for the increased neoplastic properties of *TSC2*-deficent cells via Rho signaling intermediates.

AJRCMB Articles in Press. Published November 08, 2024 as 10.1165/rcmb.2024-0111OC

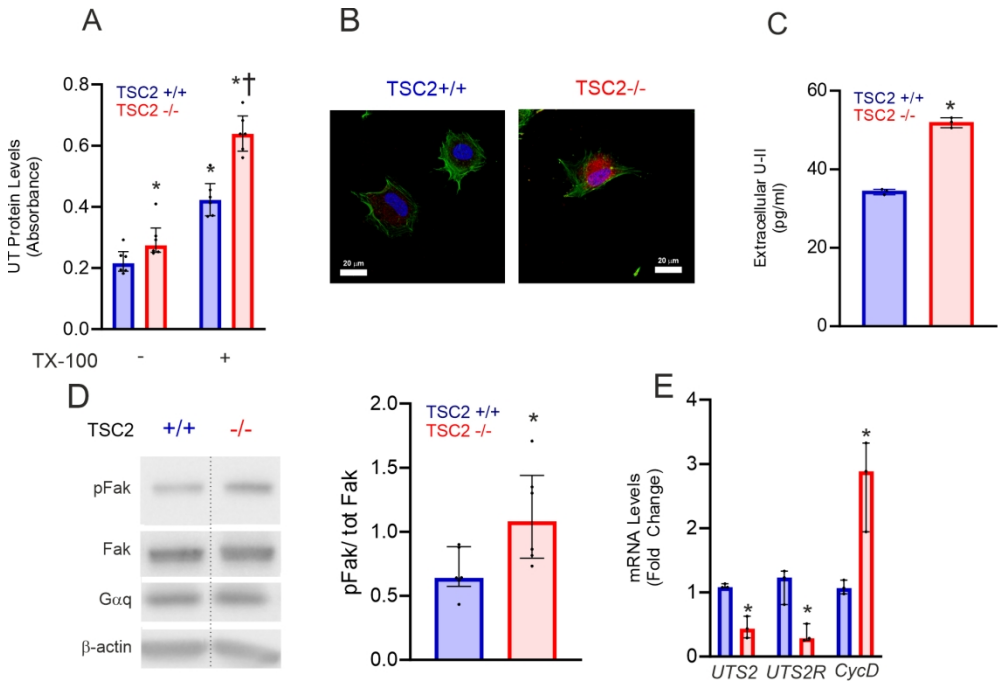

Figure 1: Urotensin-II receptor (UT) and urotensin-II (U-II) expression in LAM-SM cells

169x113mm (300 x 300 DPI)

AJRCMB Articles in Press. Published November 08, 2024 as 10.1165/rcmb.2024-0111OC

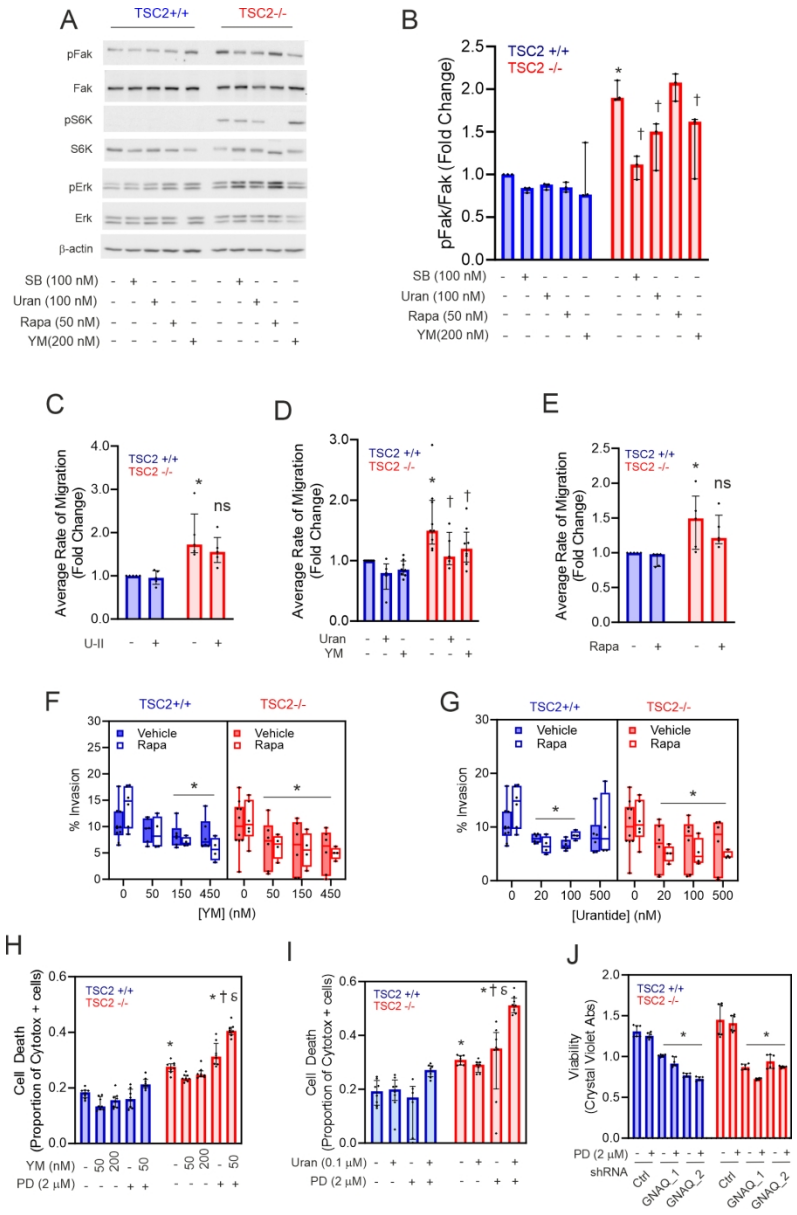

Figure 2: Neoplastic behavior of LAM-SM cells

137x209mm (300 x 300 DPI)

AJRCMB Articles in Press. Published November 08, 2024 as 10.1165/rcmb.2024-0111OC

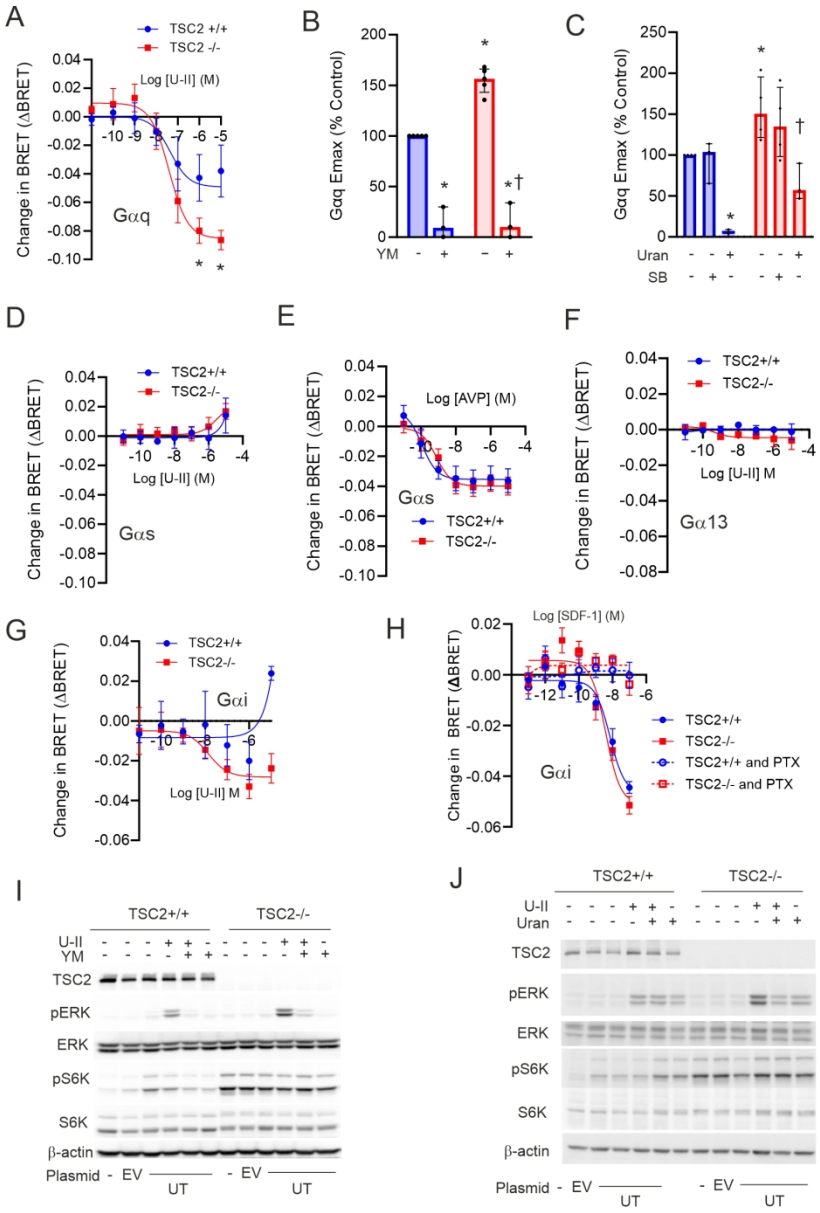

Figure 3: Effect of TSC2-deficiency on signaling by Gαq effectors in response to UT ligation

145x211mm (300 x 300 DPI)

AJRCMB Articles in Press. Published November 08, 2024 as 10.1165/rcmb.2024-0111OC

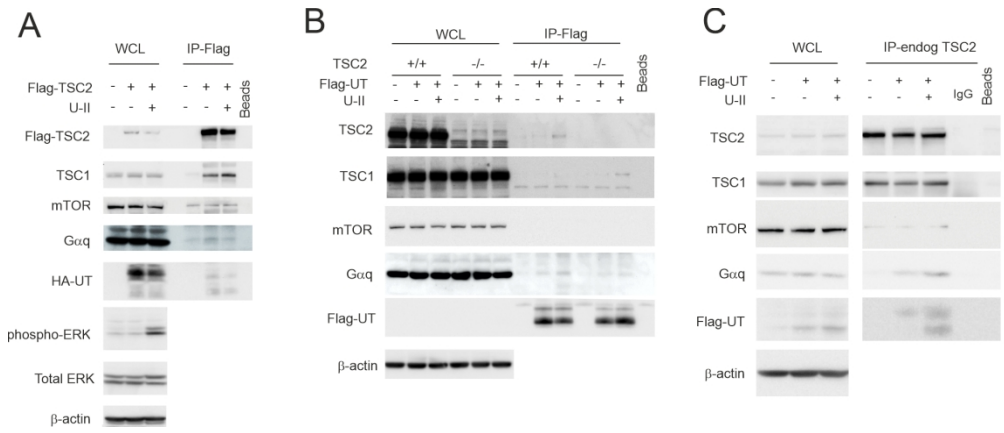

Figure 4: Physical association between TSC2, Gαq, and UT

173x72mm (300 x 300 DPI)

AJRCMB Articles in Press. Published November 08, 2024 as 10.1165/rcmb.2024-0111OC

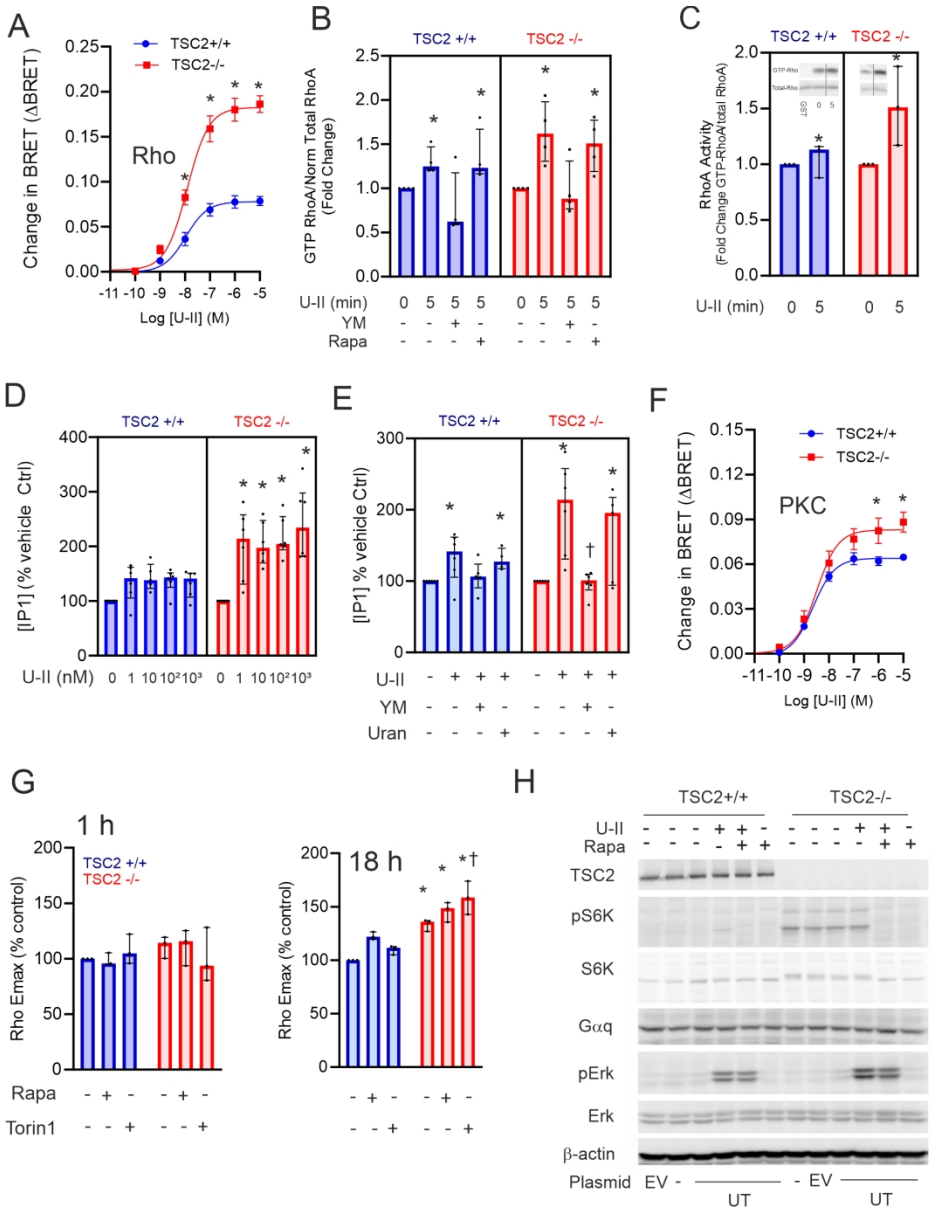

Figure 5: Effect of TSC2-deficiency on activation of Gαq downstream effectors in response to UT ligation

163x209mm (300 x 300 DPI)

AJRCMB Articles in Press. Published November 08, 2024 as 10.1165/rcmb.2024-0111OC

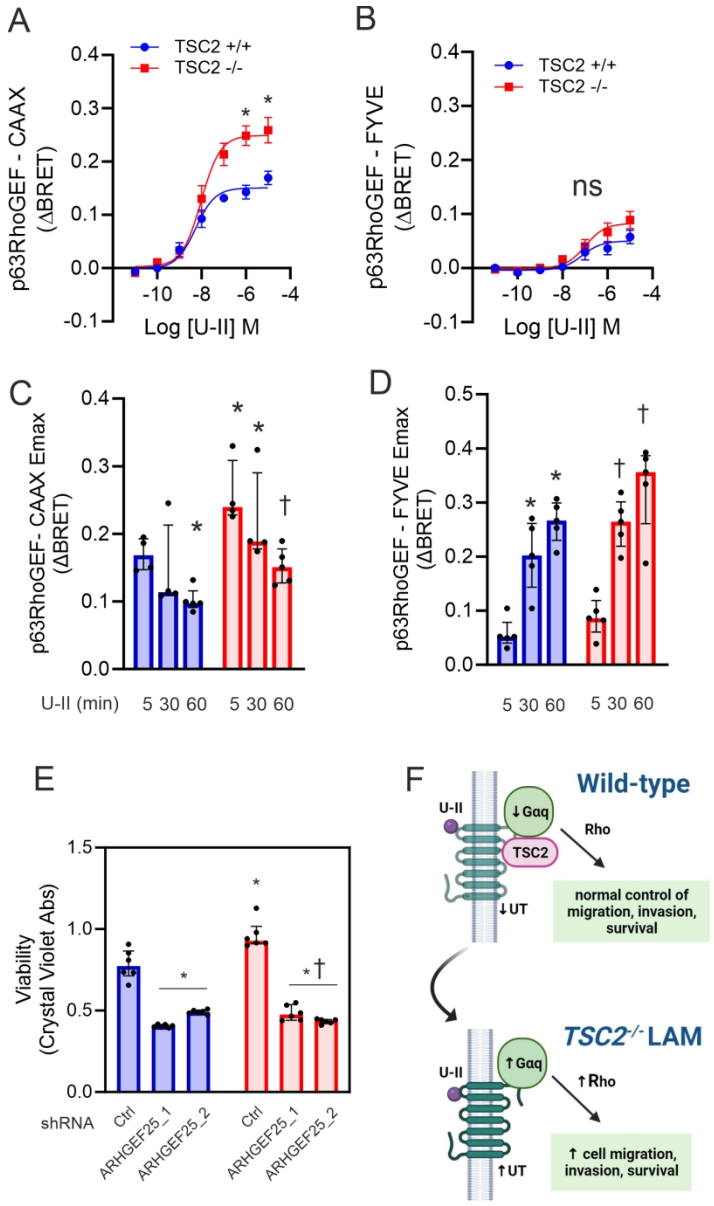

Figure. 6: Effect of TSC2-deficiency on endosomal targeting of p63RhoGEF in HEK 293T cells

125x212mm (300 x 300 DPI)

AJRCMB Articles in Press. Published November 08, 2024 as 10.1165/rcmb.2024-0111OC

Enhanced Gαq Signaling in *TSC2*-deficient Cells Is Required for Their Neoplastic Behavior

Aurelie Trefier, Nihad Tousson-Abouelazm, Lama Yamani, Sajida Ibrahim, Kwang-bo Joung, Adam Pietrobon, Julien Yockell-Lelievre, Terence E. Hébert, Reese J. Ladak, Tomoko Takano, Mark Nellist, Yoon Namkung, David Chatenet, William L. Stanford, Stephane A. Laporte, Arnold S. Kristof

ONLINE DATA SUPPLEMENT

AJRCMB Articles in Press. Published November 08, 2024 as 10.1165/rcmb.2024-0111OC

Supplemental Materials:

Table E1: Plasmids:

Expression vectors	Figure	Product	Plasmid backbone	Source
Gαq/Gβ/Gγ-Polycistronic BRET sensor	3	- Gαq -RlucII - Gβ - Gγ-GFP10	pCDNA3	Laporte lab[1]
HA-UT	3,5,6	HA-UT	pCDNA3	Laporte lab
UT-Flag	4	UT-linker-Flag	pCDNA3	Kristof lab
Flag-TSC2	4	Flag-TSC2	PRK1	Addgene #14129
GαS -RlucII	3	GαS -RlucII	pCDNA3	Laporte lab
Gα13-RlucII	3	Gαi3-RlucII	pCDNA3	Laporte lab
Gαi-RlucII	3	Gαi3-RlucII	pCDNA3	Laporte lab
Gβ1	3	Flag-Gβ1	pCDNA3	Laporte lab
Gγ2-GFP10	3	GNG2-GFP10	pCDNA3	Laporte lab
CXCR4	3	CXCR4	pCDNA3	Crepieux lab
V2R	3	HA-V2R	pCDNA3	Crepieux lab
PKN	5	Rho-binding domain in protein kinase N – see Fig. S3B	pCDNA3	Laporte lab[2]
PKC	5	Intramolecular sensor of PKC kinase activity with C-terminal C1b domain – see Fig. S3C	pCDNA3	Laporte lab[2]
P63RhoGEF-RlucII	6	Gαq-binding domain of p63RhoGEF	pCDNA3	Laporte lab[3]
CAAX-GFP10	6	Plasma membrane-targeted GFP10	pCDNA3	Laporte lab[4]
FYVE-GFP10	6	Endosomal membrane-targeted GFP10	pCDNA3	Laporte lab[4]

AJRCMB Articles in Press. Published November 08, 2024 as 10.1165/rcmb.2024-0111OC

Table E2: Chemical and peptide Reagents:

Reagent	Source	Catalogue
UII	Tocris	1642
YM-254890	Tocris	7352
PD-184252	Sigma	PZ0181
Urantide	Dr. Chatenet Lab.	Synthesized by Chatenet Lab
Rapamycin	Millipore	553210
Torin-1	Sigma	475991
SB-657510	Tocris	3571
PTX	ThermoFisher Scientific	PHZ1174
SDF-1α	Sigma-Aldrich	SRP3276
AVP	Sigma-Aldrich	V-9879
Urea	Sigma-Aldrich	U5378
DTT	ThermoFisher Scientific	20290
Digitonin	Sigma-Aldrich	D141
CHAPS	ThermoFisher Scientific	BP571-5
Protease Inhibitor cocktail	Bioshop	PIC002
Mounting solution (Aqua-mount)	Invitrogen	13800
DAPI	Thermo Scientific	62248
Alexa Fluor 488 Phalloidin	Cell Signaling Technology	8878
Phenol free Matrigel	Invitrogen	CB-40230C
Matrigel	Invitrogen	CB-40230
SigmaFast OPD Tablets	Sigma-Aldrich	P9187
Poly-L-ornithine solution	Sigma-Aldrich	P4957

AJRCMB Articles in Press. Published November 08, 2024 as 10.1165/rcmb.2024-0111OC

Table E3: Antibodies used for Western blot analysis or immunoprecipitations:

Protein/epitope	Abbreviation/GeneID	Source	Catalog number
Akt	AKT1	Cell Signaling Technology	2920S
p-Akt S473	Phosphorylated AKT1	Cell Signaling Technology	4060
Flag epitope	Flag	Millipore	F1804
Hemagglutinin epitope	HA	Millipore	05-902R
Mechanistic target of rapamycin	mTOR/MTOR	Cell Signaling Technology	2972S
p70 S6 kinase	S6K/RPS6KA1	Cell Signaling Technology	9202S
phospho-p70 S6 kinase (T389)	pS6K	Cell Signaling Technology	9205S
Beta-actin	β-actin	Sigma	A5441
G-protein αq11/14	Gαq/GNAQ	Santa-Cruz	SC-365906
G-protein α12/13	Gα13/GNA13	Santa-Cruz	SC-293424
Urotensin receptor	UT/UTS2R	Invitrogen	PA5-34299
Urotensin-II	U-II/UTS2	Mybiosource	MBS263409
RHO GTPase	RHO (A,B,C) clone 55	Millipore	05-778
Mitogen-activated protein kinase Erk-1 and 2	ERK1/2	Cell Signaling Technology	9102S
Mitogen-activated protein kinase Erk-1 and 2	p-ERK1/2	Cell Signaling Technology	4370S
Focal adhesion Kinase	FAK	BD Tranduction Laboratories	610088
p-Focal adhesion Kinase (Y397)	p-FAK Y397	Cell Signaling Technology	3283S
Tuberin (Rabbit)	TSC2	Cell Signaling Technology	3612S
Tuberin (Mouse)	TSC2	Invitrogen	37-0500
Hamartin	TSC1	Cell Signaling Technology	6935S
Normal Rabbit IgG		Cell Signaling Technology	2729
Peroxidase-conjugated AffiniPure Goat Anti-Mouse IgG		Jackson ImmunoResearch Laboratories	115-005-003
Peroxidase-conjugated AffiniPure Goat Anti-Rabbit IgG		Jackson ImmunoResearch Laboratories	111-035-003
Anti-Flag M2 affinity beads	Flag	Sigma-Aldrich	M8823
Goat anti-rabbit IgG Secondary Antibody, Alexa Fluor 647		Invitrogen	A-21245
Pureproteome Protein A Magnetic Bead system		Millipore	LSKMAGA02

AJRCMB Articles in Press. Published November 08, 2024 as 10.1165/rcmb.2024-0111OC

Table E4A: Oligonucleotide primers (5'-3') for Sybr Green-based Real-time PCR:

Transcript	Forward Primer	Reverse Primer
UTS2R	CAACGCAACCCTCAACAGC	CCGACAGCAGAGTCCCAATG
GAPDH	GGCCAAAGCAAAGAGACGTG	GGCCAAAGCAAAGAGACGTG
UTS2	CAGCCCTAAACACAGCATGG	GGCCAAAGCAAAGAGACGTG
Cyclin D	AGCTGTGCATCTACACCGAC	GAAATCGTGCGGGGTCATTG

Table E4B: Oligonucleotide primers (5'-3') for cloning of Flag-UTS2R:

Plasmid	Forward Primer	Reverse Primer	Template
PCDNA3-UTS2R-linker Flag*	tacggcaAAGCTTatggcgctgaccccgagtc	taattaGGATCCtgatgatcctgatgatcccgccggggccctgggaccct	PCDNA3-UTS2R-Flag

*See supplemental methods for cloning procedure.

AJRCMB Articles in Press. Published November 08, 2024 as 10.1165/rcmb.2024-0111OC

Table E5: shRNAs and their targeted sequences:

Transcript	Lentiviral shRNA	Sigma designation	Targeted sequence
UTS2R	UTS2R	TRCN0000014465	GCTCACCAGGAACTACCGCGA
ARHGEF25	ARHGEF_1	TRCN0000021609	CGGTGTCTGAAAGATCCTGAT
ARHGEF25	ARHGEF_2	TRCN0000021610	GCTCTGGAAAGGAGTATGTAT
GNAQ	GNAQ_1	TRCN0000036459	CGACCTGGAGAACATCATCTT
GNAQ	GNAQ_2	TRCN0000036463	CGACAGCGACAAGATCATCTA
None	Non-targeting	SHC016	GCGCGATAGCGCTAATAATTT

AJRCMB Articles in Press. Published November 08, 2024 as 10.1165/rcmb.2024-0111OC

Table E6: Effect of inhibitors on PKN and PKC activity:

	TSC2$^{+/+}$		*TSC2*$^{-/-}$	
	Ctrl	YM-254890	Ctrl	YM-254890
PKN	100	18 (16, 31)*	228 (226, 273)*	38 (22, 47)†
PKC	100	5 (3,15)*	118 (110,125)*	6 (5,19)†
	Ctrl	Urantide	Ctrl	Urantide
PKN	100	40 (26,44)*	190 (143,229)*	51 (34,59)†
PKC	100	52 (47,52)*	123 (116,125)*	61 (51,72)†
	Ctrl	PD-184352	Ctrl	PD-184352
PKN	100	97 (87, 100)	155 (154, 180)	156 (134, 177)
PKC	100	94 (76, 98)	109 (94, 124)	116 (111, 135)
	Ctrl	PTX	Ctrl	PTX
PKN	100	107 (79, 167)	152 (115, 184)*	125 (104, 164)

TSC2$^{+/+}$ or *TSC2*$^{-/-}$ HEK 293T cells expressing the RhoA (PKN) or protein kinase C (PKC) BRET reporters were exposed to vehicle (Ctrl), the Gαq inhibitor YM-254890 (200 nM), the UT inhibitor urantide (100 nM), the MEK inhibitor PD-184352 (2 μM), or the Gαi inhibitor pertussis toxin (PTX; 100 ng/ml) for 1 h prior to addition of U-II at the concentration indicated in Figures 5A and F. Shown are the medians of Emax values normalized to vehicle treated controls = 100% with interquartile range in parentheses (n=3-5 experiments). *p < 0.05 vs. *TSC2*$^{+/+}$ vehicle treated control, †p<0.05 *vs.* *TSC2*$^{-/-}$ vehicle treated control.

AJRCMB Articles in Press. Published November 08, 2024 as 10.1165/rcmb.2024-0111OC

Table E7: Effect of Gαq inhibitor on p63RhoGEF membrane localization:

Time (min)	5				30				60			
	TSC2$^{+/+}$		*TSC2*$^{-/-}$		*TSC2*$^{+/+}$		*TSC2*$^{-/-}$		*TSC2*$^{+/+}$		*TSC2*$^{-/-}$	
YM-254890	-	+	-	+	-	+	-	+	-	+	-	+
p63 RhoGEF CAAX	100	11 (5,13)*	151 (135,164)*	1.1 (0.4,1.3†	100	6 (2, 26)*	174 (129, 185)*	3 (2, 9)†	100	25 (22, 27)*	135 (134, 152)*	14 (6, 23)†
p63 RhoGEF FYVE	100	30 (3, 36)*	161 (105, 180)*	34 (2, 54)†	100	10 (3, 13)*	133, (116, 145)*	2 (0.2, 6.7)†	100	6 (3, 15)*	122 (116, 152)*	3 (0, 8)†
	TSC2$^{+/+}$		*TSC2*$^{-/-}$		*TSC2*$^{+/+}$		*TSC2*$^{-/-}$		*TSC2*$^{+/+}$		*TSC2*$^{-/-}$	
PTX	-	+	-	+	-	+	-	+	-	+	-	+
p63 RhoGEF CAAX	100	103 (100,121)	151 (135,164)*	158 (154,161)	100	92 (69m 106)	174 (129, 185)*	124 (102, 166)	100	107 (97, 123)	135 (134, 156)*	117 (105, 137)
p63 RhoGEF FYVE	100	77 (51, 87)	161 (105, 180)*	140 (128, 157)	100	98 (89, 103)	133 (116, 145)*	133 (121, 141)	100	100 (94, 101)	122 (116, 152)*	120 (105, 121)

TSC2$^{+/+}$ or *TSC2*$^{-/-}$ HEK 293T cells expressing the p63RhoGEF plasma membrane (CAAX) or endosomal membrane (FYVE) BRET reporter systems were exposed to vehicle, the Gαq inhibitor YM-254890 (200 nM) or the Gαi inhibitor pertussis toxin (PTX; 100 ng/ml) overnight prior to addition of U-II at the concentration indicated in Figures 6A and B for 5, 30, or 60 min before initiation of BRET. Shown are the medians of Emax values normalized to vehicle treated controls = 100% with interquartile range in parentheses (n=3-6 experiments). *$p < 0.05$ vs. *TSC2*$^{+/+}$ vehicle treated control, †$p<0.05$ *vs.* *TSC2*$^{-/-}$ vehicle treated control.

AJRCMB Articles in Press. Published November 08, 2024 as 10.1165/rcmb.2024-0111OC

Supplemental Methods:

Cell Culture:

HEK293 cells were cultured in DMEM supplemented with or without 10% FBS in the presence of penicillin, 100U/ml, and streptomycin, 100 µg/ml. Parental (TSC2+/+) or knockout (TSC2-/-) were obtained from the Tuberous Sclerosis Alliance (Silver Springs, Marland) via the Van Andel Research Institute (Grand Rapids, Michigan). The *TSC2* gene was deleted by CRSPR/Cas9 gene editing and validated by RNAseq analysis (Fig. E2). Unless otherwise indicated, 1 x 10^6 HEK 293T cells were plated and, after recovery, transfected with the indicated mammalian expression vectors, or plasmids for expression of BRET sensors, using calcium phosphate/DNA precipitates; cells were then incubated for 24 h in complete medium prior to initiation of experimental protocols. To achieve equal amounts of total plasmid (10 µg) for transfections, expression vectors were supplemented using an appropriate amount of empty vector.

The engineering of human pluripotent stem cell-derived *TSC2*$^{-/-}$ cells (LAM-SM cells) and *TSC2*$^{+/+}$ controls was previously described in detail[5]. LAM-SM cells were differentiated from *TSC2* CRISPR/Cas9 knockout (*TSC2*$^{-/-}$) female cells using smooth muscle differentiation medium[5,6]. The cells were maintained in smooth muscle growth media in Matrigel, 0.16 mg/ml, with Media231 supplemented with SMGS 25% (Gibco) and 0.1% Gentamycin (Wisent Bioproducts). These cells and their *TSC2*$^{+/+}$ SM controls were also engineered to constitutively express mCherry protein in the AAVS1 safe harbor locus by CRISPR/Cas9 gene editing for their detection during imaging. Cells were grown on.

ELISA:

UII ELISA: Sandwich ELISA was conducted on media supernatants using a UII ELISA kit (MyBioSource, USA, Cat.no: MBS762653). Briefly, 100 uL of prepared standards (UII, 0-1000 pg/mL) or media supernatant samples were added to wells pre-coated with anti-UII and incubated for 90 min at 37ºC. Following rinsing, 100 uL of Biotin-labelled anti-UII primary antibody, diluted at 1:100, was added to each well and incubated for 60 min at 37ºC. After rinsing three times, 100uL of secondary antibody, conjugated to HRP-Streptavidin diluted to 1:100, was added to the occupied wells and incubated for 30 min at 37ºC. Following five washes, tetramethylbenzidine substrate and stop solutions were added. The TECAN Infinite Pro 200 plate reader (absorbance wavelength: 450nm) was used to measure the optical density (OD) values. Concentrations of UII were derived by interpolation of OD values using the standard curve.

In cell UT ELISA: Cells were seeded (50,000 cells/well) using 96 well plate coated with polyornithine for transfected HEK293T cells or Matrigel for LAM-SM cells. After 24 h, media was aspirated, and wells were washed with PBS (with 1 mM $MgCl_2$ and 1mM $CaCl_2$) before fixation with 3% paraformaldehyde (PFA) in PBS for 10 min at room temperature. After washing with PBS, 0.5% Triton in PBS was added to designated wells for 5 min at RT. Cells were then washed 3 times with wash buffer (0.5% BSA in PBS) and incubated for 1 hr at RT. Wells were then incubated with primary antibody (1:1000 anti-UT (Fig. 1) or anti-HA (Fig. E2C) at RT for 1 hr before washing 3 times with wash buffer and incubation with peroxidase-conjugated anti-rabbit IgG secondary antibody for 1h at RT. OPD Fast Substrate was added, and the TECAN Infinite Pro 200 plate reader (absorbance wavelength: 450nm) was used to measure optical density (OD).

AJRCMB Articles in Press. Published November 08, 2024 as 10.1165/rcmb.2024-0111OC

RhoA G-LISA: (*TSC2*$^{+/+}$) or knockout (*TSC2*$^{-/-}$) HEK293T cells transfected with UT-HA-pCDNA3 or pCDNA3 empty vector were used for the study, and assays were performed using RhoA G-LISA kit (Cytoskeleton, Inc., cat# BK124). Cells were serum starved in phenol free DMEM for 18 h and the indicated drugs were added prior to stimulation with 10 nM U-II for 5 min. Cells were then lysed using the supplied buffer and cleared by centrifugation at 10,000 x g for 1 min at 4^{o}C. Protein levels for each sample were measured as per the kit instructions and equalized to a concentration of 1 ug/ul using lysis buffer. GTP bound RhoA level was subsequently measured using 25 ul of lysate per sample in duplicate according to manufacturer's protocol. Optical densities were detected by measuring absorbance at 490 nm using a TECAN Infinite Pro 200 plate reader.

Pull-down assay for active RhoA:

Preparation of GST-fused Rho binding domain of Rhotekin (GST-RBD), which binds active (GTP-bound) RhoA was described previously[7]. Whole cell lysates containing 1 mg protein were incubated with purified GST-RBD or GST alone each bound to glutathione sepharose beads for 1 h at 4°C. Before incubation with beads, aliquots of the whole cell lysates were saved for evaluation of total RhoA levels. The beads were washed twice before addition of Laemmli buffer. Whole cell (total) RhoA and GST-RBD-purified RhoA were separated by SDS-PAGE before detection of RhoA levels by Western blot.

Confocal microscopy

35 mm dishes with microscope slide coverslips were coated with Matrigel (1:60 in serum free phenol free media). 30,000 *TSC2*$^{+/+}$ or $^{-/-}$ cells were added per well for 5 h before rinsing and fixation with 4% PFA for 15 min. Plates were then bleached overnight at 4^{o}C under white light before rinsing and permeabilization with 0.1% Triton X-100 in PBS for 20 min at room temperature. After rinsing with 1% BSA in PBS, rabbit anti-UT antibody was added for 1 h at room temperature followed by rinsing and addition of Alexa 647-conjugated goat anti-rabbit and Alexa 488-conjugated Phalloidin for 1 h at room temperature. Coverslips were mounted on microscope slides using Aqua-mount solution (Invitrogen) with DAPI. Images were acquired using confocal laser-scanning microscope (LSM 780, Zeiss, Germany) with excitation at 488 nm and 647 nm, equipped with Plan-Apochromat 40X/1.4 oil immersion DIC M27 objective lens. We gathered the autofluorescence spectrum on a non-labeled specimen to eliminate autofluorescence noise.

Western bot analysis:

Upon termination of experimental conditions, cells were washed twice with ice-cold PBS and exposed to NP40 lysis buffer (20 mM Tris HCL PH 8, 50 mM NaF, 1mM EDTA, 100 µM Na_3VO_4, 1% NP-40, protease inhibitor cocktail (Bioshop, 10 ul/ml)) for 30 minutes at 4°C with gentle rocking. Lysates were centrifuged at 20,000 g for 15 min at 4°C, and proteins in the supernatant were measured by colorimetric assay (*DC* Protein Assay, Bio-RAD). For SDS-PAGE, Laemmli buffer was added to lysates adjusting for equal amounts of protein, and samples were separated electrophoretically before transfer of proteins to polyvinylidene fluoride membranes (0.2 µm pore size). Membranes were washed and incubated with primary antibody in with 5% BSA at 4 °C overnight. Membranes were washed and incubated for 1 h at room temperature with horseradish peroxidase- conjugated secondary antibody. Bands were detected using an enhanced chemiluminescence kit and imaged. Quantitative densitometry was performed using ImageJ.

AJRCMB Articles in Press. Published November 08, 2024 as 10.1165/rcmb.2024-0111OC

Immunoprecipitation:
Upon termination of experimental conditions, cells were washed twice with ice-cold PBS and exposed to CHAPS lysis buffer (20 mM Tris HCL PH 8, 50 mM NaF, 0.3% CHAPS, 10 mM β glycerophosphate, 1mM EDTA, 100 μM Na_3VO_4 and protease inhibitor cocktail) for 30 minutes at 4°C with gentle rocking. Lysates were centrifuged at 16,000 g for 10 minutes, and supernatants were incubated with anti-M2-Flag affinity beads (for Flag-fused proteins) or anti-TSC2 antibody (for endogenous TSC2) overnight at 4 °C followed by incubation with and Protein A magnetic beads for 20 min at room temperature. Beads were washed three times with CHAPS lysis buffer, and proteins were eluted from the beads with urea sample buffer (6 M urea, 2% SDS, 50mM Tris PH 6.8, glycerol 20%, 200 mM DTT) while incubating at room temperature for 2 h with shaking. For Flag-UT immunoprecipitations, the cell lysates were split prior to incubation with anti-M2-flag affinity beads and washed beads were incubated with urea sample buffer containing 1% digitonin for solubilization and recovery of Flag-UT, or Laemmli buffer to preserve the prey proteins. Equal amounts of sample buffer were subjected to Western blot analysis as indicated above.

Cloning of Flag UT expression construct used in in immunoprecipitation: We first cloned the UTS2R cDNA into a pCDNA3 plasmid for insertion of cDNAs upstream of a Flag-encoding sequence followed by a stop codon (Addgene, #20011) for the expression of c-terminal Flag-fused UT. Although the encoded protein could be expressed in HEK 293T cells, ligand-activated signaling (*i.e.*, U-II activated phosphorylation of ERK) was absent. Using this construct as template, we therefore amplified the UT-expressing cDNA with primers (see Table E4B) to incorporate BamH1 and HindIII restriction sites, as well as a 7 amino acid linker/insert (GSSGSSS) between the C-terminus of UT and the Flag epitope. After expression of the PCDNA3-UT-linker-Flag product, ERK phosphorylation in response to U-II was intact. This Flag-UT construct was used for experiments in Fig. 4B and C.

Scratch assay:
A mono-layer scratch assay using the IncuCyte live cell imaging system was performed. This assay measures scratch closure by real time high content imaging with automated calculation of 'wound confluence' at each time point. 40,000 cells per well were seeded on a 96-well ImageLock plate (Essen BioScience, United States) previously coated with Matrigel (50 ul/well). Adhered cells were starved in serum free DMEM for 16 h and a scratch wound was performed using a 96-pin Wound Maker (WoundMaker, Essen BioScience). After creating the scratch, the medium was aspirated, and the wells were washed twice with fresh medium to remove any cells from the scratched area. Following the washes, 100 μL of media without or with the indicated concentration so of agonists or inhibitors was added to each well. Wells were imaged every 2h for 12h using the 10x objective. The images were analyzed using the IncuCyte scratch wound analysis software and the migration of cells was quantified using the wound confluence (%), which is defined as the percentage of the wound region area occupied by cells.

Cytotoxicity and cell viability assays:
Cytotox green staining. To determine the cytotoxicity of YM-254890, urantide, or PD-184252 (PD) alone or in combination, IncuCyte ® Cytotoxicity Assay (Essen BioScience Inc., Ann Arbor,

AJRCMB Articles in Press. Published November 08, 2024 as 10.1165/rcmb.2024-0111OC

MI) was performed as per the manufacturer's instructions. Briefly, $TSC2^{-/-}$ LAM-SM and $TSC2^{+/+}$ control cells, which were engineered to express mCherry, were seeded into a 96-well plate at a density of 2 x 10^4 cells per well. Following serum starvation overnight, medium containing vehicle or the indicated agonists or inhibitors were added to the cells together with 250 nM IncuCyte® Cytotox Green Reagent (Essen BioScience Inc.). LAM-SM cells were cultured and imaged every 2h for 48h. Dead cells were identified by detecting green fluorescence using IncuCyte® software (Essen BioScience Inc.). The data were expressed as Cytotox+ cells as a proportion of total cells (mCherry+).

Crystal violet staining. Cells were washed once in PBS before staining with 0.05% Crystal violet solution for 5 minutes. Cells were then washed 3 times with PBS, before solubilization in 1% SDS. Crystal violet staining, as an index of cell viability, was measured by absorption spectrophotometry (λ = 570nm).

Lentiviral vector production and transduction:

Two million HEK 293T cells were seeded in a T25 flask before transfection with PLKO-shRNA plasmid and packaging vectors (Sigma) by calcium phosphate precipitation. Briefly, plasmids (6 ug PLKO-shRNA, 1.5 ug pMDLg/pREE, 1.5 ug pRSV-Rev, 3 ug pMD2-VSVG were added to 220 ul of distilled H_2O, before addition of 31 ul of 2M $CaCl_2$, and mixing. Distilled water was then added for a DNA/CaCl2 mixture of 500 ul, which was added dropwise to 500 ul of 2x HBS (50 mM HEPES, 280 mM NaCl, 1.5 mM Na_2HPO_4). After incubation for 20 min at room temperature, the precipitate mixture was added dropwise to the T25 flask containing 5 ml of fresh medium, and incubated overnight at 37°C, before replacing with fresh media. After 24 h, culture supernatants were subjected to filtering (45 uM). The virus-containing medium was overlaid on a 10% sucrose-containing buffer (50 mM Tris-HCl, pH 7.4,100 mM NaCl, 0.5 mM EDTA) at a 4:1 v/v ratio and centrifuged at 10,000 x g at 4 °C for 4h. After centrifugation, the supernatant was carefully removed, and the tube was placed on the tissue paper for 3 minutes. PBS, 2 ml, was added to the semi-dried tube for re-suspension, and the purified virus was aliquoted and kept at -80 °C until use. Viral particles were quantified using the One Wash™ Lentivirus Titer Kit (OriGene, #TR30038). We applied 1 x 10^6 Transduction Units (~1 x 10^4 pg virus) per ml of culture media over 48 to 72 h for viral transductions.

BRET:

HEK 293 cells were seeded at a density of 1.10^6 cells per 100 mm dishes and grown in complete medium (DMEM supplemented with 10% v/v FBS, 100 U/ml penicillin, and 0.1 mg/ml streptomycin). Next day, cells were transiently transfected by calcium phosphate coprecipitation. Briefly, Plasmid for expression of HA-UT, along with biosensor plasmids and empty vector for a total of 10 µg DNA were mixed in a solution containing 125 mM $CaCl_2$ in HEPES-buffered saline [25 mM HEPES (pH 7.4), 140 mM NaCl, 0.75 mM Na_2HPO_4] for 5 min, and the mixed solution was then added to cells. After 24 h, cells were detached and seeded onto poly-ornithine-coated 96-well white plates at a density of 50,000 cells per well in media. The next day, cells were washed once with Tyrode's buffer (140 mM NaCl, 2.7 mM KCl, 1 mM CaCl2, 12 mM $NaHCO_3$, 5.6 mM D-glucose, 0.5 mM $MgCl_2$, 0.37 mMNaH_2PO_4, 25 mM HEPES, pH 7.4). BRET signals were monitored using a Synergy2 (BioTek) microplate reader after adding coelenterazine 400a (5 µM) for 3 min, followed by the addition of various concentrations of ligands for 2-5 min. The filter set

AJRCMB Articles in Press. Published November 08, 2024 as 10.1165/rcmb.2024-0111OC

was 410/80 nm and 515/30 nm for detecting the RlucII (Renilla luciferase)(donor) and GFP10 (acceptor) light emissions, respectively. BRET ratios were determined by dividing emission intensities of light from GFP10 divided by the those from light emitted by the RlucII.

AJRCMB Articles in Press. Published November 08, 2024 as 10.1165/rcmb.2024-0111OC

References

1. Namkung, Y., Radresa, O., Armando, S., Devost, D., Beautrait, A., Le Gouill, C., and Laporte, S.A. (2016). Quantifying biased signaling in GPCRs using BRET-based biosensors. *Methods* **92**, 5
2. Namkung, Y., LeGouill, C., Kumar, S., Cao, Y., Teixeira, L.B., Lukasheva, V., Giubilaro, J., Simoes, S.C., Longpre, J.M., Devost, D., Hebert, T.E., Pineyro, G., Leduc, R., Costa-Neto, C.M., Bouvier, M., and Laporte, S.A. (2018). Functional selectivity profiling of the angiotensin II type 1 receptor using pathway-wide BRET signaling sensors. *Sci Signal* **11**
3. Avet, C., Mancini, A., Breton, B., Le Gouill, C., Hauser, A.S., Normand, C., Kobayashi, H., Gross, F., Hogue, M., Lukasheva, V., St-Onge, S., Carrier, M., Heroux, M., Morissette, S., Fauman, E.B., Fortin, J.P., Schann, S., Leroy, X., Gloriam, D.E., and Bouvier, M. (2022). Effector membrane translocation biosensors reveal G protein and betaarrestin coupling profiles of 100 therapeutically relevant GPCRs. *Elife* **11**
4. Namkung, Y., Le Gouill, C., Lukashova, V., Kobayashi, H., Hogue, M., Khoury, E., Song, M., Bouvier, M., and Laporte, S.A. (2016). Monitoring G protein-coupled receptor and beta-arrestin trafficking in live cells using enhanced bystander BRET. *Nat Commun* **7**, 12178
5. Pietrobon, A., Yockell-Lelievre, J., Melong, N., Smith, L.J., Delaney, S.P., Azzam, N., Xue, C., Merwin, N., Lian, E., Camacho-Magallanes, A., Dore, C., Musso, G., Julian, L.M., Kristof, A.S., Tam, R.Y., Berman, J.N., Shoichet, M.S., and Stanford, W.L. (2023). Tissue-Engineered Disease Modeling of Lymphangioleiomyomatosis Exposes a Therapeutic Vulnerability to HDAC Inhibition. *Adv Sci (Weinh)*, e2302611
6. Pietrobon, A., Yockell-Lelievre, J., Flood, T.A., and Stanford, W.L. (2022). Renal organoid modeling of tuberous sclerosis complex reveals lesion features arise from diverse developmental processes. *Cell Rep* **40**, 111048
7. Sander, E.E., ten Klooster, J.P., van Delft, S., van der Kammen, R.A., and Collard, J.G. (1999). Rac downregulates Rho activity: reciprocal balance between both GTPases determines cellular morphology and migratory behavior. *J Cell Biol* **147**, 1009

AJRCMB Articles in Press. Published November 08, 2024 as 10.1165/rcmb.2024-0111OC

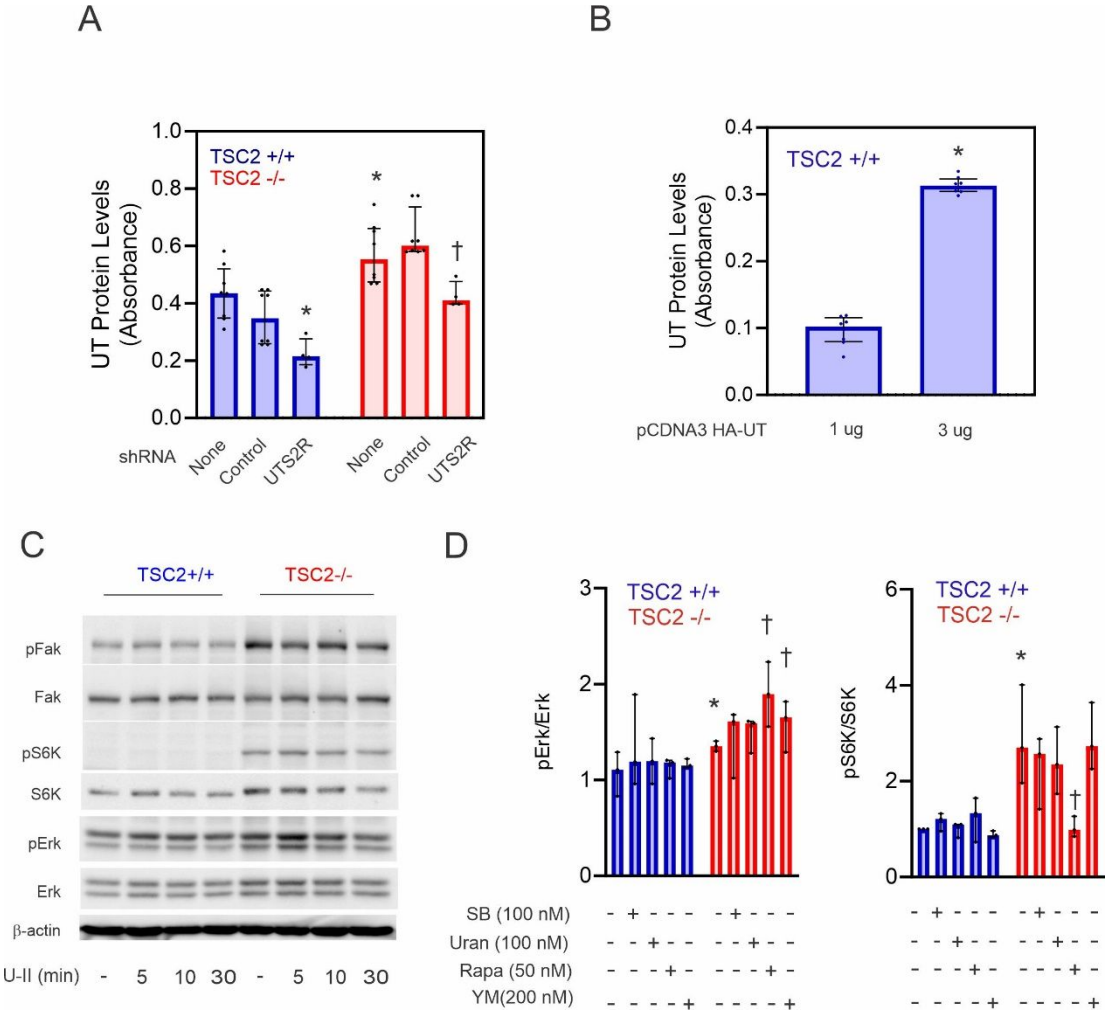

Figure E1: UT Expression and activity in LAM-SM cells: A. LAM-SM cells (*TSC2*$^{-/-}$) or wild-type controls were subjected to transduction with no virus (none) or lentiviral vectors for the expression of scrambled non-targeting shRNAs (Control) or those targeting UT-encoding mRNA (*UTS2R*) before evaluation of UT protein levels by in cell ELISA using anti-UT antibody. Shown are the medians of octuplet absorbance values ± interquartile range from two experiments. **B.** HEK 293T cells were transfected with empty plasmid vector, or 1 or 3 ug/ml of plasmid for the expression of recombinant HA-fused UT before detection of UT protein by in cell ELISA using anti-UT antibody. Shown are medians of absorbance values above empty vector control in octuplet samples ± interquartile range representative of two experiments. **C.** LAM-SM cells (*TSC2*$^{-/-}$) or wild-type SM controls were deprived of serum for 18 h before incubation with 10 nM urotensin-II (U-II) for the indicated times, and interrogation of whole cell lysates for the indicated proteins. **D.** Quantification of phospho- and total ERK and S6K band densitometry for western blots described in Figure 2A. Data are medians of band density for phospho-ERK (pERK) to total ERK ratios or phospho-S6K (pS6K) to total S6K ratios ± interquartile range . *p<0.05 *vs.* vehicle-treated TSC2$^{+/+}$ control. †p<0.05 *vs.* vehicle-treated TSC2$^{-/-}$ control.

AJRCMB Articles in Press. Published November 08, 2024 as 10.1165/rcmb.2024-0111OC

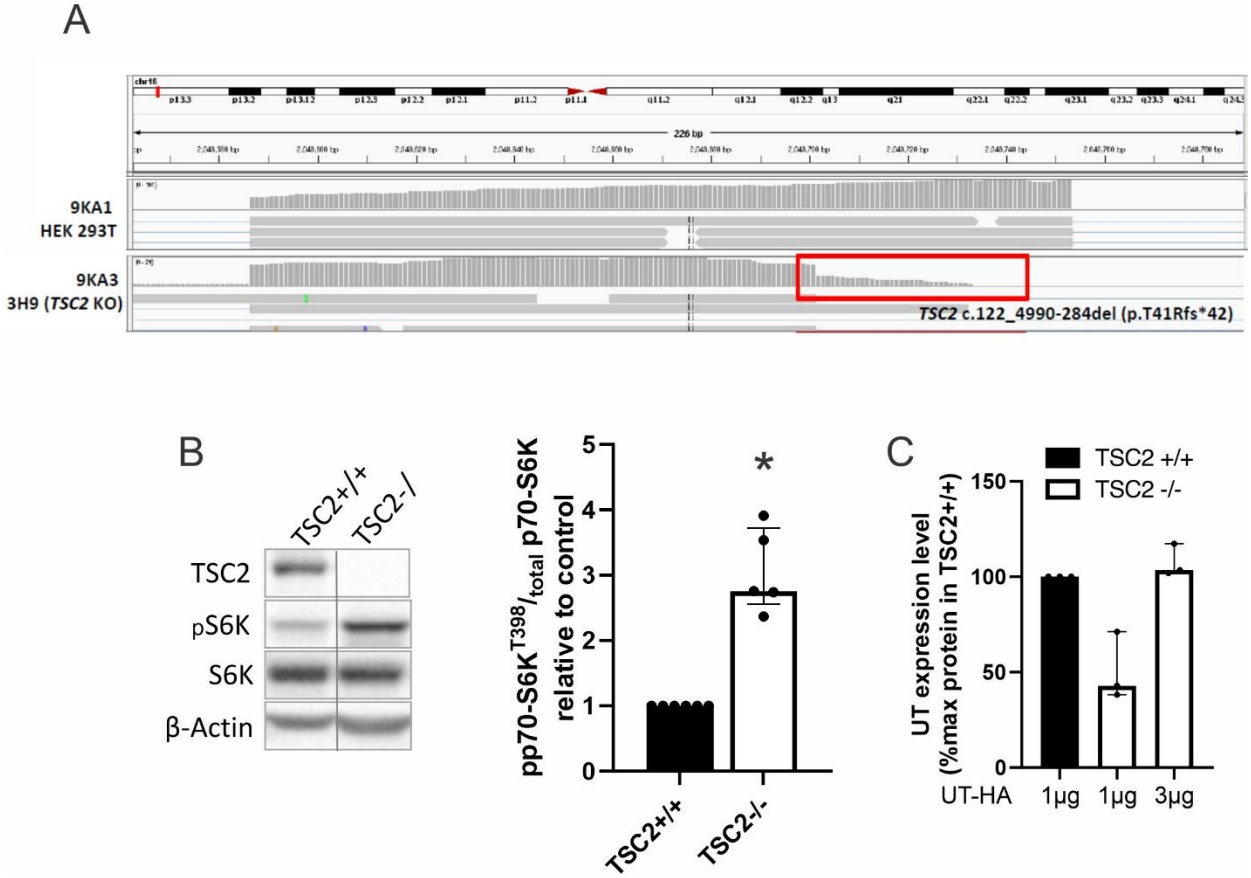

Figure E2: UT expression in HEK 293T cells: CRISPR/Cas9-mediated genome-editing was used to eliminate expression from HEK293 cells of the *TSC2* gene. **A.** Shown are mapped results of next generation sequencing (RNAseq) from $TSC2^{+/+}$ (9KA1 HEK 293T) or $TSC2^{-/-}$ (9KA3 3H9 KO) cells indicating loss of *TSC2* transcript, leading to **B.** loss of TSC2 protein expression and elevated p70 S6 Kinase activity. **C.** Dose-dependent expression of recombinant HA-UT in $TSC2^{+/+}$ or $TSC2^{-/-}$ cells as detected by in cell ELISA using anti-HA antibody. Data in B. and C. are the medians of fold change in band density or absorbance from 3-5 experiments normalized to $TSC2^{+/+}$ cells ± interquartile range. *p<0.05 *vs.* $TSC^{+/+}$ control.

AJRCMB Articles in Press. Published November 08, 2024 as 10.1165/rcmb.2024-0111OC

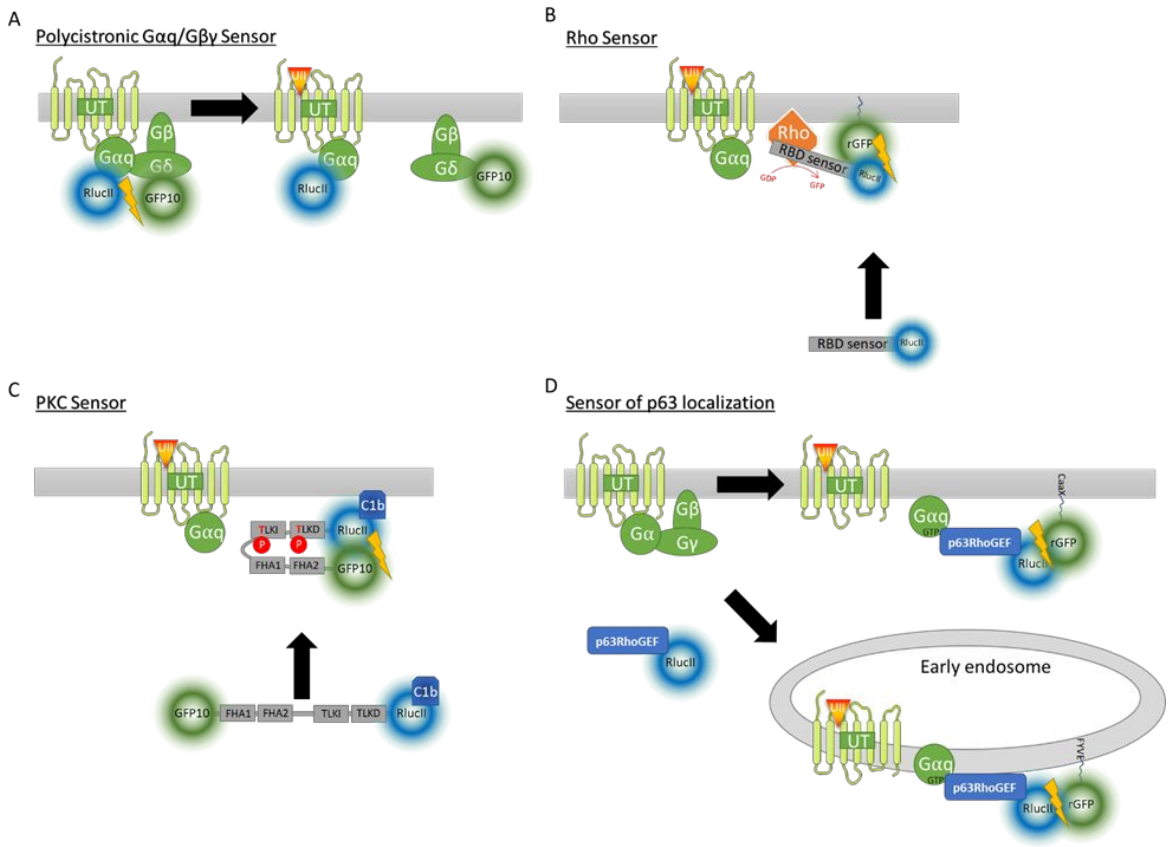

Figure E3: Description of BRET-based biosensors: BRET constructs are detailed in Table E1. **A-C:** Upon incubation with urotensin-II (UII; red triangle), activation of the Gαq isoform is reflected by its dissociation from Gβγ (**A**), resulting in reduced BRET signal. Gαq-RlucII was co-expressed with Flag-Gβ and Gγ-GFP10 from a polycistronic expression plasmid. For Gαs, Gα13, and Gαi isoforms, their RlucII fusion products were co-expressed with Flag-Gβ and Gγ-GFP10 from separate plasmids. **B.** The Rho biosensor contains the Rho binding domain (RBD) of protein kinase N fused to RlucII and is co-expressed with rGFP fused to a membrane targeting domain (CAAX). **C.** The protein kinase C (PKC) biosensor contains the PKC consensus phospho-threonine binding domains (FHA1 and 2) and two threonine in the TLKI and TLKD domains of PKC. Upon phosphorylation, the threonine residues bind their binding domains; this causes a conformational change that leads to proximity between GFP10 and RlucII and a BRET signal. **D.** The Gαq-binding domain of p63RhoGEF was fused to RlucII (p63RhoGEF-RlucII) and co-expressed with the plasma membrane targeting sequence CAAX or the endosome targeting FYVE domain each fused to rGFP. Optimization of detection of FYVE-rGFP activation by p63RhoGEF required the simultaneous co-expression of unfused recombinant Gαq. This biosensor is therefore a reporter of Gαq-mediated activation of p63RhoGEF at the plasma membrane or the endosome.

AJRCMB Articles in Press. Published November 08, 2024 as 10.1165/rcmb.2024-0111OC

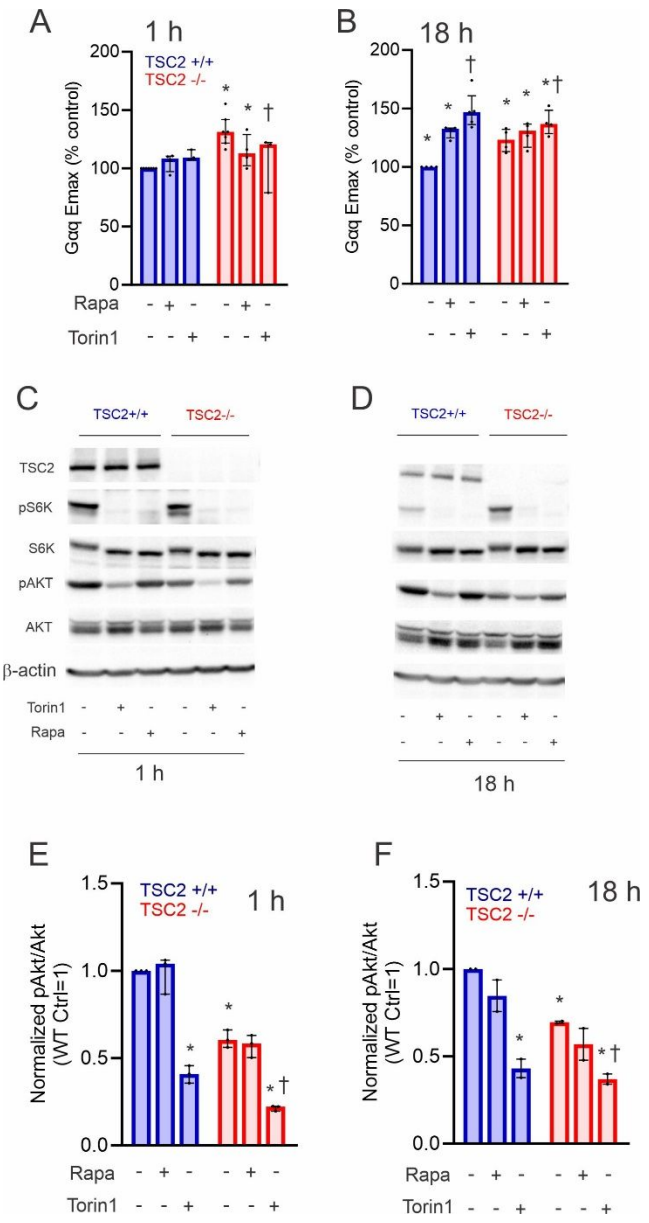

Figure E4: Effect of mTOR blockade on Gαq activity: A. and **B.** Maximum Gαq biosensor activation (Emax) by U-II in **A.** short (1h) or **B.** long term (18h) exposure to the mTORC1 inhibitor rapamycin (Rapa; 50nM) or the mTORC1/2 inhibitor Torin1 (50nM). BRET measurements were recorded and normalized to the response of U-II in the same experiment and expressed as %Emax *vs.* *TSC2*$^{+/+}$ cells = 100%. Data are medians ± inter-quartile range of three independent experiments. **C-D.** *TSC2*$^{+/+}$ or *TSC2*$^{-/-}$ HEK 293T cells were exposed to rapamycin (Rapa; 50nM) or Torin1 (50nM) for 1 or 18h before preparation of whole cell lysates and detection of phospho-AKT (pAKT) at S473 and phospho-p70 S6 kinase (pS6K) at T389. **E-F.** Shown are the medians of pAKT divided by total AKT band densities normalized to vehicle-treated *TSC2*$^{+/+}$ controls = 1 ± interquartile range from 3 experiments. *p<0.05 *vs.* vehicle treated *TSC2*$^{+/+}$ control, †p<0.05 *vs.* vehicle treated *TSC2*$^{-/-}$ control.

AJRCMB Articles in Press. Published November 08, 2024 as 10.1165/rcmb.2024-0111OC

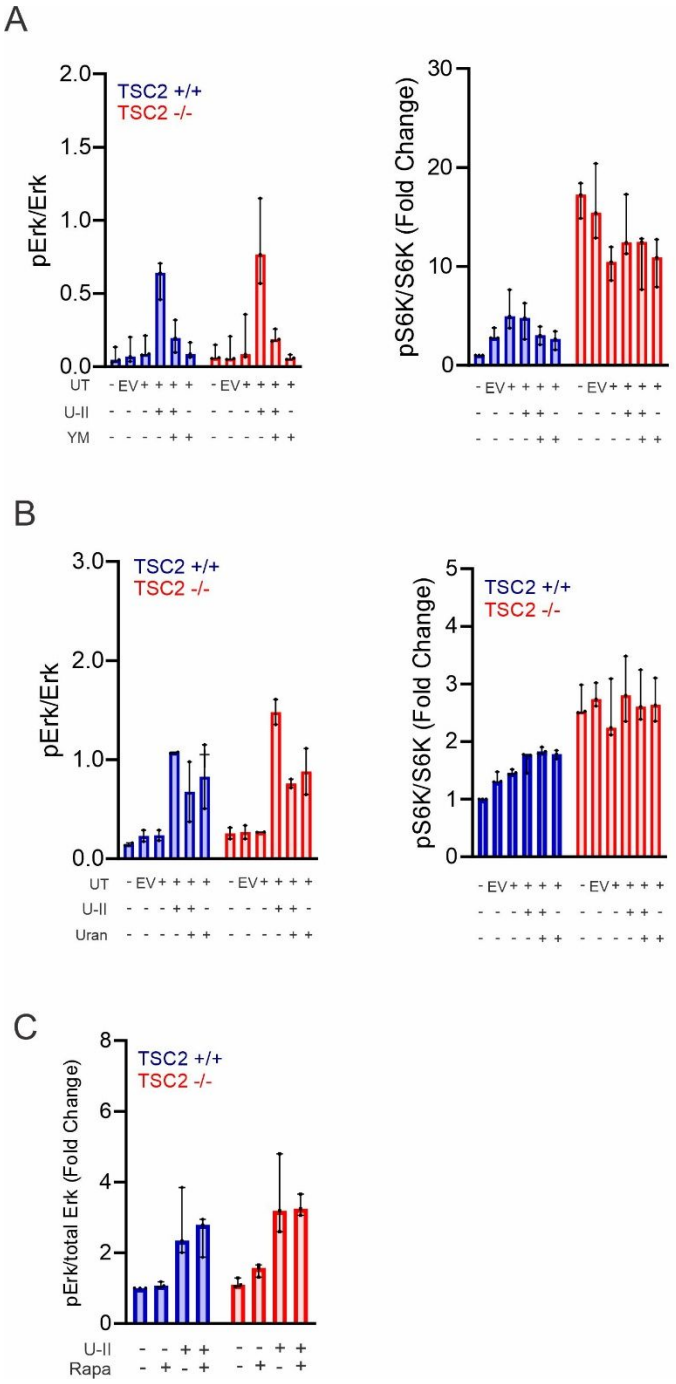

Figure E5: Effect of Inhibitors on U-II-induced activation of ERK. A. - C. *TSC2*$^{+/+}$ or *TSC2*$^{-/-}$ cells were transfected with plasmids expressing recombinant UT before exposure to its agonist U-II (10 nM), the Gαq inhibitor YM-254890 (YM; 200 nM) or the UT inhibitor urantide (Uran; 100 nM) before detection of the indicated proteins by western blot analysis and measurement of phospho-Erk T202/Y204 (pErk) and total Erk (Erk) levels by band densitometry, or phospho-p70 S6 kinase T389 (pS6K) and total p70 S6 kinase (S6K). Data are the medians of phospho- to total protein ratios or those normalized to vehicle-treated *TSC2*$^{+/+}$ controls = 1 ± interquartile range.

AJRCMB Articles in Press. Published November 08, 2024 as 10.1165/rcmb.2024-0111OC

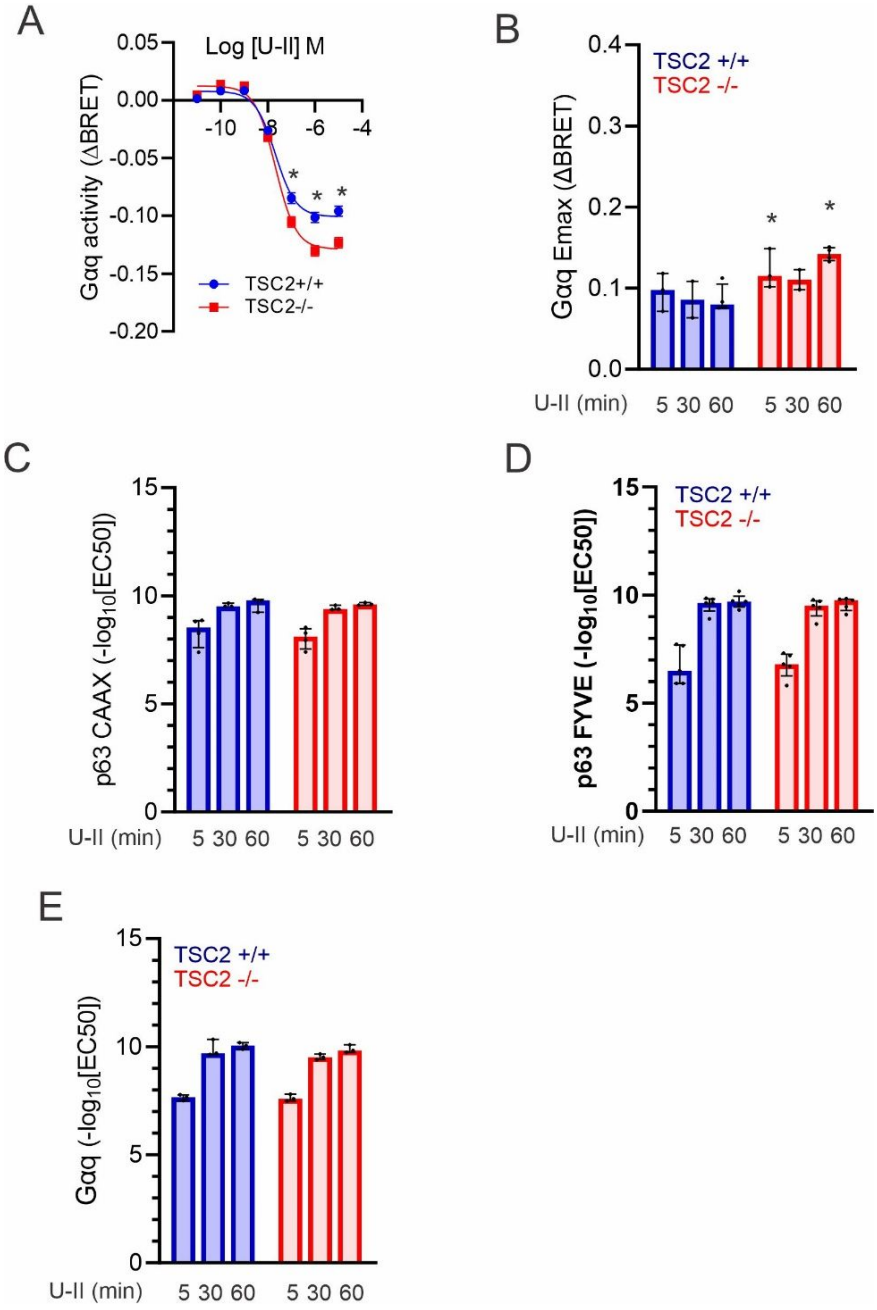

Figure E6: Recruitment of Gαq and p63RhoGEF to plasma membrane and endosomal compartments: A.-E. *TSC2*$^{+/+}$ or *TSC2*$^{-/-}$ cells were co-transfected with plasmids for the expression of HA-UT and BRET reporters for **A.** and **B.** Gαq activity (Fig. E3A), **C.** Plasma membrane recruitment of p63RhoGEF (see Fig. E3D) (*i.e.*, RlucII-fused p63RhoGEF and rGFP-CAAX), or **D.** endosomal membrane recruitment of p63RhoGEF (*i.e.*, RlucII-fused p63RhoGEF and rGFP-FYVE) before generation of urotensin-II (U-II) concentration-response relationships. Shown in **B.-E.** are the means of EC_{50} for U-II stimulation of p63RhoGEF at the (C) plasma membrane or (D) endosome ± SEM, and the medians of (B) Emax and (E) EC_{50} for stimulation of Gαq activity ± interquartile range from 3-5 experiments. *p<0.05 vs. *TSC2*$^{+/+}$ control.

AJRCMB Articles in Press. Published November 08, 2024 as 10.1165/rcmb.2024-0111OC